

The Importance of Flavor in SMEFT Electroweak Precision Fits

Luigi Bellafronte,^{1,*} Sally Dawson,^{2,†} and Pier Paolo Giardino^{1,‡}

¹*Instituto Galego de Física de Altas Enerxías, Universidade de Santiago de Compostela,
15782 Santiago de Compostela, Galicia, Spain*

²*High Energy Theory Group, Department of Physics, Brookhaven National Laboratory, Upton, NY 11973, USA*

Effective field theory tools are essential for exploring non-Standard Model physics at the LHC in the absence of the discovery of new light particles. Predictions for observables are typically made at the lowest order in the QCD and electroweak expansions in the Standard Model effective field theory (SMEFT) and often ignore the effects of flavor. Here, we present results for electroweak precision observables (EWPOs) at the next-to-leading order QCD and electroweak expansions (NLO) of the SMEFT with an arbitrary flavor structure for the fermion operators. Numerical NLO SMEFT fits to EWPOs have a strong dependence on the assumed flavor structures and we demonstrate this using various popular assumptions for flavor symmetries.

arXiv:2304.00029v2 [hep-ph] 10 May 2023

* Electronic address: lui.bellafronte@usc.es

† Electronic address: dawson@bnl.gov

‡ Electronic address: pierpaolo.giardino@usc.es

I. INTRODUCTION

The high luminosity (HL) LHC program will greatly improve our knowledge of the allowed possibilities for physics beyond the Standard Model (SM). In the absence of the discovery of a new particle, the Standard Model Effective Field Theory (SMEFT) is the tool of choice for describing new physics effects and provides a point of comparison with Standard Model (SM) predictions[1, 2]. The SMEFT is constructed as an expansion in higher dimension operators, with the $SU(3) \times SU(2) \times U(1)$ gauge symmetry unbroken,

$$\mathcal{L} = \mathcal{L}_{SM} + \sum_{k=5}^{\infty} \sum_{a=1}^{\Sigma^n} \frac{C_a^k}{\Lambda^{k-4}} \mathcal{O}_a^k. \quad (1)$$

The operators of mass-dimension k , \mathcal{O}_a^k , are constructed from SM fields and all of the effects of the beyond the SM (BSM) physics reside in the coefficient functions, C_a^k . In a UV complete model, these coefficients will be predicted at the high scale Λ [3–6]. The comparison between the SMEFT and the SM predictions thus requires SM predictions to the highest possible accuracy, along with SMEFT calculations beyond the leading order (LO). LO calculations in the SMEFT are automated[7, 8] as are NLO QCD SMEFT calculations [9], but electroweak corrections must be performed on a case by case basis.

There exist numerous global fits comparing SMEFT predictions with electroweak precision, di-boson, Higgs, and top quark observables[10–14]. However, given the large number of SMEFT operators, it is impossible to do a fully general fit. The SMEFT theory predictions thus encode various assumptions, including the termination of the SMEFT expansion at some order in $1/\Lambda^2$, the loop order of the QCD and electroweak expansions, and the flavor structure of fermion operators, among others. Understanding the uncertainties inherent in these assumptions is crucial for interpreting SMEFT fits[15].

The assumptions about the flavor structure introduce significant model dependence into the SMEFT predictions. It is straightforward to implement a general flavor structure for the tree level predictions for observables[16–22] and the one-loop \overline{MS} renormalization of the dimension-6 coefficient functions is known for an arbitrary flavor structure[23–25]. The one-loop next-to-leading order (NLO) electroweak predictions for physical observables, however, typically involve a large number of 4-fermion and 2-fermion operators with potentially complicated flavor structures. In addition, the fermion operators introduce new subtleties in the renormalization procedure. Existing calculations of the one-loop electroweak corrections to EWPO, Higgs, and di-boson data do not include the most general flavor structure for the 2- quark and 4- quark operators in the loops[26–32]. Here, we generalize our previous NLO SMEFT calculation of EWPOs[33–35] which included 4-fermion operators, but not 2-fermion operators, to allow for an arbitrary flavor structure. The corrections to the EWPOs from 4-fermion operators in the $U(3)^5$ symmetric case are in [31]. The role of flavor assumptions in fits to top and bottom quark data has been extensively examined in the literature and those analyses are complementary to that presented here[35–38].

We set the CKM matrix to be diagonal, which implies that only operators containing pairs of identical flavor fermions contribute. We further work to linear order in the SMEFT coefficients and set all masses other than the top quark to be 0. We want to remark that these two conditions constrain the light fermion Yukawa couplings to be zero, without additional assumptions, since the SMEFT operators that would induce a modification to the SM Yukawas do not interfere with the SM amplitudes at linear order.

In Section II, we review the SMEFT framework and the role of flavor assumptions. Here we construct the general form of the 2-fermion and 4-fermion coefficients that occur in the one-loop computations of EWPOs corresponding to different flavor ansatz. We describe the NLO electroweak and QCD renormalization of EWPOs in detail in Section III with emphasis on the roles of the 2- and 4-fermion operators. Section IV contains phenomenology results and demonstrates the important role of flavor assumptions in the SMEFT fits[39]. We see that even including more general flavor assumptions than earlier analyses, many blind directions remain in the fits. Finally, Section V contains some conclusions. Numerical results for the EWPOs, along with $H \rightarrow Z\gamma$ and $H \rightarrow \gamma\gamma$, with arbitrary flavor structures at NLO in the SMEFT are contained in supplemental material.

II. SMEFT

Our calculations are done using the dimension-6 SMEFT Lagrangian and the Warsaw basis[40]. Retaining only the dimension-6 operators (and dropping the superscript k), we calculate observables, O_b , to one-loop as an expansion in $\frac{1}{\Lambda^2}$ and keep only the linear terms since the SMEFT is renormalizable order by order in powers of $\frac{1}{\Lambda^2}$,

$$O_b = O_{b,SM} + \sum_{a=1}^n \frac{C_a}{\Lambda^2} \beta_{ab}, \quad (2)$$

where β_{ab} is process dependent and depends on the kinematic invariants and the input parameters, and $O_{b,SM}$ is the SM prediction. The dimension-6 SMEFT framework is described in detail in the literature, and here we review only those aspects relevant to the current calculations. We use the Feynman rules from Ref. [2], with general flavor structures for the 2- and 4-fermion operators, although we assume that the CKM matrix is diagonal, which has implications for the fermion structures of the operators that contribute to our calculation, as we will see. Furthermore, we assume that the SMEFT does not introduce new sources of CP violation, that is we assume the coefficients of all the operators to be real.

Our goal is the dimension-6 SMEFT calculation of NLO QCD and NLO electroweak corrections to electroweak precision observables (EWPOs) with arbitrary flavor structures for the operators involving fermions. The technical details are in the next section and in the following sub-sections we discuss the effects of flavor on the predictions.

In the following, fermion fields are written using the notation

$$\begin{aligned} (q^i)^T &= (\bar{u}_L^i, \bar{d}_L^i) & u^i &= u_R, c_R, t_R \\ (l^i)^T &= (\bar{\nu}_L^i, \bar{e}_L^i) & d^i &= d_R, s_R, b_R \\ & & e^i &= e_R, \mu_R, \tau_R, \end{aligned} \quad (3)$$

with $i = 1, 2, 3$ the generation (flavor) index. Moreover, we define the Higgs doublet as

$$\phi = \begin{pmatrix} \varphi^+ \\ \frac{1}{\sqrt{2}}(v + h + i\varphi^0) \end{pmatrix}, \quad (4)$$

where h , φ^+ and φ^0 are the Higgs and Goldstone bosons, and v is the electroweak vacuum expectation value.

A. EWPO

In complete generality, the Warsaw basis contains 2499 baryon number conserving dimension-6 operators. Much of the proliferation of operators is associated with the flavor structure. Of course, most of the flavor structures will not contribute to a given observable and we begin by considering EWPOs at tree level. The Z and W boson pole observables that we consider are,

$$M_W, \Gamma_W, \Gamma_Z, \sigma_h, R_e, R_\mu, R_\tau, R_s, R_c, R_b, A_e, A_\mu, A_\tau, A_s, A_c, A_b, A_{e,FB}, A_{\mu,FB}, A_{\tau,FB}, A_{FB,s}, A_{FB,c}, A_{FB,b}. \quad (5)$$

Note that we do not use the effective mixing angle in our fits, since it is derived from the asymmetries.

The operators that contribute to the EWPOs at LO are comprised of two bosonic operators with no flavor structure ($O_{\phi WB}$ and $O_{\phi D}$) and 8 fermionic operators, of which there are 7 operators with 2 fermionic indices (the 2-fermion operators), and 1 operator with 4 fermionic indices (the 4-fermion operator). The explicit forms of the operators that appear at LO are reported in Table I. These operators change the couplings of the Z and W bosons to fermions, and explicit predictions for the measured quantities of Eq. 5 are given in Appendix A of Ref. [27]. The only 4-fermion operator that is relevant for EWPOs at LO is $\mathcal{O}_l[ijkl]$ which has the symmetry $\mathcal{O}_l[ijkl] = \mathcal{O}_l[klij]$ and only $\mathcal{O}_l[2112] = \mathcal{O}_l[1221]$ contributes to the observables of Eq.5. The indices ($i, j, k, l = 1, 2, 3$) refer to the fermion

$\mathcal{O}_{ll}[ijkl]$	$(\bar{l}_i \gamma_\mu l_j)(\bar{l}_k \gamma^\mu l_l)$	$\mathcal{O}_{\phi WB}$	$(\phi^\dagger \tau^a \phi) W_{\mu\nu}^\alpha B^{\mu\nu}$	$\mathcal{O}_{\phi D}$	$(\phi^\dagger D^\mu \phi)^* (\phi^\dagger D_\mu \phi)$
$\mathcal{O}_{\phi e}[ij]$	$(\phi^\dagger iD_\mu \phi)(\bar{e}_{Ri} \gamma^\mu e_{Rj})$	$\mathcal{O}_{\phi u}[ij]$	$(\phi^\dagger iD_\mu \phi)(\bar{u}_{Ri} \gamma^\mu u_{Rj})$	$\mathcal{O}_{\phi d}[ij]$	$(\phi^\dagger iD_\mu \phi)(\bar{d}_{Ri} \gamma^\mu d_{Rj})$
$\mathcal{O}_{\phi q}^{(3)}[ij]$	$(\phi^\dagger iD_\mu^\alpha \phi)(\bar{q}_i \tau^a \gamma^\mu q_j)$	$\mathcal{O}_{\phi q}^{(1)}[ij]$	$(\phi^\dagger iD_\mu \phi)(\bar{q}_i \tau^a \gamma^\mu q_j)$	$\mathcal{O}_{\phi l}^{(3)}[ij]$	$(\phi^\dagger iD_\mu^\alpha \phi)(\bar{l}_i \tau^a \gamma^\mu l_j)$
$\mathcal{O}_{\phi l}^{(1)}[ij]$	$(\phi^\dagger iD_\mu \phi)(\bar{l}_i \tau^a \gamma^\mu l_j)$				

Table I. Dimension-6 operators contributing to the Z and W pole observables of this study at tree level. $i, j, k, l = 1, 2, 3$ are generation indices. We define $\phi^\dagger iD_\mu \phi = i\phi^\dagger (D_\mu \phi) - i(D_\mu \phi)^\dagger \phi$ and $\phi^\dagger iD_\mu^\alpha \phi = i\phi^\dagger \tau^a D_\mu \phi - i(D_\mu \phi)^\dagger \tau^a \phi$.

generation.) Dimension-6 operators involving the electron and the muon give contributions to the decay of the μ , changing the relation between the vev, v , and the Fermi constant G_μ ,

$$G_\mu \equiv \frac{1}{\sqrt{2}v^2} - \frac{1}{\sqrt{2}\Lambda^2} \mathcal{C}_{ll}[1221] + \frac{1}{\sqrt{2}\Lambda^2} \left(\mathcal{C}_{\phi l}^{(3)}[11] + \mathcal{C}_{\phi l}^{(3)}[22] \right). \quad (6)$$

At NLO, the EWPOs of Eq. 5 receive contributions from 22 additional operators (which are defined in Ref. [27]), which we classify according to the number of fermions:

- 4 bosonic operators:

$$\mathcal{O}_{\phi B}, \mathcal{O}_{\phi W}, \mathcal{O}_\square, \mathcal{O}_W. \quad (7)$$

- 2 2-fermion operators:

$$\mathcal{O}_{uB}[ij], \mathcal{O}_{uW}[ij]. \quad (8)$$

Notice that only $\mathcal{O}_{uB}[33]$ and $\mathcal{O}_{uW}[33]$ contribute to the EWPOs at NLO if all fermions except the top are massless.

- 16 4-fermion operators:

$$\begin{aligned} & \mathcal{O}_{ed}[ijkl], \mathcal{O}_{ee}[ijkl], \mathcal{O}_{eu}[ijkl], \mathcal{O}_{lu}[ijkl], \mathcal{O}_{ld}[ijkl], \mathcal{O}_{le}[ijkl], \mathcal{O}_{lq}^{(1)}[ijkl], \mathcal{O}_{lq}^{(3)}[ijkl] \\ & \mathcal{O}_{qe}[ijkl], \mathcal{O}_{qd}^{(1)}[ijkl], \mathcal{O}_{qq}^{(3)}[ijkl], \mathcal{O}_{qq}^{(1)}[ijkl], \mathcal{O}_{qu}^{(1)}[ijkl], \mathcal{O}_{ud}^{(1)}[ijkl], \mathcal{O}_{uu}[ijkl], \mathcal{O}_{dd}[ijkl]. \end{aligned} \quad (9)$$

Five of the NLO-generated 4-fermion operators have a flavor symmetry,

$$\mathcal{O}_{ee}[ijkl], \mathcal{O}_{qq}^{(3)}[ijkl], \mathcal{O}_{qq}^{(1)}[ijkl], \mathcal{O}_{uu}[ijkl], \mathcal{O}_{dd}[ijkl] \equiv \mathcal{O}_Y[ijkl] = \mathcal{O}_Y[klij]. \quad (10)$$

It is convenient to categorize the operators according to their dependence on the flavor since only specific structures contribute to the EWPOs at NLO:

- A) 2-fermion operators: $\mathcal{O}_X[ij] \equiv \mathcal{O}_{\phi e}[ij], \mathcal{O}_{\phi u}[ij], \mathcal{O}_{\phi d}[ij], \mathcal{O}_{\phi q}^{(3)}[ij], \mathcal{O}_{\phi q}^{(1)}[ij], \mathcal{O}_{\phi l}^{(3)}[ij], \mathcal{O}_{\phi l}^{(1)}[ij], \mathcal{O}_{uB}[ij], \mathcal{O}_{uW}[ij]$. We consider the CKM matrix to be diagonal which has the consequence that the coefficients of the operators in Class A have diagonal flavor structures:

$$\mathcal{C}_X[ij] = E_X^{(i)} \delta_{ij}, \quad i, j = 1, 2, 3, \quad (11)$$

resulting in 3 independent coefficients for each operator. Notice that the operator $\mathcal{O}_{\phi u}[33]$ first contributes to the EWPOs at NLO. Furthermore, as noted above, $\mathcal{O}_{uB}[ij]$ and $\mathcal{O}_{uW}[ij]$ enter in our calculations only with coefficients $\mathcal{C}_{uB}[33]$ and $\mathcal{C}_{uW}[33]$ respectively. Together there are 23 independent coefficients in Class A.

- B) 4-fermion operators involving only identical fermion representations: $\mathcal{O}_Y[ijkl] \equiv \mathcal{O}_{ee}[ijkl], \mathcal{O}_{qq}^{(3)}[ijkl], \mathcal{O}_{qq}^{(1)}[ijkl], \mathcal{O}_{uu}[ijkl], \mathcal{O}_{dd}[ijkl], \mathcal{O}_{ll}[ijkl]$. Since they stem from the combination of two fermion currents belonging to identical representations once we require that the CKM matrix is the unit matrix, there are only two ways flavor is allowed to "flow" through these operators: $\mathcal{O}_Y[iijj]$ and $\mathcal{O}_Y[ijjj]$. Furthermore, these operators are subject to the flavor symmetry in Eq. 10, resulting in the coefficients having the flavor structure,

$$\begin{aligned} \mathcal{C}_Y[iiii] &= F_Y^{(i)}, \mathcal{C}_Y[iijj] = A_Y^{(ij)}, \mathcal{C}_Y[ijjj] = B_Y^{(ij)}, \\ A_Y^{(ji)} &= A_Y^{(ij)}, B_Y^{(ji)} = B_Y^{(ij)}, \quad i \neq j \text{ \& } i, j = 1, 2, 3, \end{aligned} \quad (12)$$

resulting in 9 independent coefficients for each operator. However, the flavor structure of $\mathcal{O}_{ee}[ijkl]$ is further constrained by the Fiertz identity $(\bar{e}_i \gamma^\mu e_j)(\bar{e}_k \gamma^\mu e_l) = (\bar{e}_i \gamma^\mu e_l)(\bar{e}_k \gamma^\mu e_j)$, which imposes the equality $A_{ee}^{(ij)} = B_{ee}^{(ij)}$, reducing the number of independent coefficients for $\mathcal{O}_{ee}[ijkl]$ to 6. The only coefficient of Class B that does not contribute to the EWPOs at NLO is $\mathcal{C}_{uu}[3333]$. In total, we have 50 independent coefficients in Class B contributing.

- C) 4-fermion operators with 2 different fermion representations: $\mathcal{O}_Z[ijkl] \equiv \mathcal{O}_{ed}[ijkl], \mathcal{O}_{eu}[ijkl], \mathcal{O}_{lu}[ijkl], \mathcal{O}_{ld}[ijkl], \mathcal{O}_{le}[ijkl], \mathcal{O}_{lq}^{(1)}[ijkl], \mathcal{O}_{lq}^{(3)}[ijkl], \mathcal{O}_{qe}[ijkl], \mathcal{O}_{qd}^{(1)}[ijkl], \mathcal{O}_{qu}^{(1)}[ijkl], \mathcal{O}_{ud}^{(1)}[ijkl]$. For these operators, our choice of a diagonal CKM matrix requires that the flavor must flow only in one way: $\mathcal{O}_Y[iijj]$. Therefore, the coefficients of these operators have the flavor structure:

$$\mathcal{C}_Z[iijj] = D_Z^{(ij)}, \quad i, j = 1, 2, 3, \quad (13)$$

with no further restrictions, corresponding to 9 independent coefficients for each operator, for a total of 99 independent coefficients in Class C that contribute to the observables of Eq. 5 at NLO.

In the most general flavor case, we see that EWPOs computed to NLO receive contributions from 178 independent coefficients: 6 from bosonic operators, 23 from 2-fermion operators, and 149 from 4-fermion operators. We next consider different flavor assumptions for the fermionic operators in order to reduce the number of operators that need to be considered. The flavor assumptions we consider are $U(3)^5$, minimal flavor violation (MFV), $U(2)^5$, third generation centric, third generation phobic, third generation phobic + $U(2)^5$, and a flavorless structure. We will discuss each of these assumptions in detail in the following sub-sections.

B. Flavor Assumptions: $U(3)^5$

In the absence of Yukawa couplings, the SM fermions have a global $U(3)^5$ symmetry,

$$G_3 \equiv U(3)_q \times U(3)_l \times U(3)_u \times U(3)_d \times U(3)_e. \quad (14)$$

The introduction of Yukawa interactions in the SM Lagrangian preserves a global hypercharge symmetry $U(1)_Y$, a baryonic symmetry $U(1)_B$, and three leptonic symmetries, $U(1)_e$, $U(1)_\mu$ and $U(1)_\tau$.

Our first approximation when imposing flavor symmetries on SMEFT predictions is to assume that the dimension-6 SMEFT coefficients have the G_3 symmetry of the (Yukawa-less) SM. This symmetry prevents the generation of the operators $\mathcal{O}_{uW}[33]$ and $\mathcal{O}_{uB}[33]$ since they carry a left-right fermionic current.

Under G_3 , the other operators in Class A respect the form

$$\text{Class A : } \mathcal{C}_X[ii] = E_X, \quad i = 1, 2, 3, \quad (15)$$

All the 2-fermion operators that contribute to the EWPOs automatically have the structure of Eq. 15, and there are 7 real coefficients in this class, consistent with the counting of Ref. [19].

Regarding the operators of Class B, both contractions of fermion indices

$$(\bar{f}_i \gamma^\mu f_i)(\bar{f}_j \gamma^\mu f_j), \quad (\bar{f}_i \gamma^\mu f_j)(\bar{f}_j \gamma^\mu f_i), \quad (16)$$

are invariant under $U(3)^5$, so the coefficients of Class B reduce to

$$\text{Class B : } \mathcal{C}_Y[iiii] = A_Y + B_Y, \mathcal{C}_Y[iijj] = A_Y, \mathcal{C}_Y[ijji] = B_Y, \quad i \neq j \text{ \& } i, j = 1, 2, 3. \quad (17)$$

Remembering that $B_{ee} = A_{ee}$, there are 11 independent coefficients in Class B.

Finally, the operators in Class C have the structure

$$\text{Class C : } \mathcal{C}_Z[iijj] = D_Z \quad i, j = 1, 2, 3, \quad (18)$$

for a total of 11 independent coefficients also in Class C. In total, if we impose a G_3 symmetry on the SMEFT Lagrangian, we are left with 29 independent coefficients contributing to the EWPOs at one loop.¹

C. Flavor Assumptions: MFV

The Yukawa couplings break the $U(3)^5$ global symmetry in the SM. If we assume that this is the *only* source of breaking of the G_3 symmetry, we are led to the MFV scenario²[41]. The SM Yukawa couplings are considered as $U(3)^5$ auxiliary fields with the transformations,

$$\begin{aligned} Y_u &\sim (3, 1, \bar{3}, 1, 1) \\ Y_d &\sim (3, 1, 1, \bar{3}, 1) \\ Y_e &\sim (1, 3, 1, 1, \bar{3}). \end{aligned} \quad (19)$$

It is always possible to choose a basis such that Y_u , Y_d , and Y_e are diagonal matrices. We remind the reader that we have assumed that the CKM matrix is diagonal and the only non-zero fermion mass is assumed to be the top quark mass, M_t . The coefficients of the operators containing at least 2 top quarks are modified, while the other coefficients retain the G_3 structure. Our implementation of the MFV scenario with a massless b quark is equivalent to a global $U(2)_q \times U(3)_l \times U(2)_u \times U(3)_d \times U(3)_e$ symmetry.

In Class A, the only operators with a flavor structure that depends on the third generation fermions are $\mathcal{O}_{\phi u}$, $\mathcal{O}_{\phi q}^{(3)}$, $\mathcal{O}_{\phi q}^{(1)}$, \mathcal{O}_{uW} and \mathcal{O}_{uB} .

$$\begin{aligned} \text{Class A : } \mathcal{C}_X[\alpha\alpha] &= E_X, \mathcal{C}_X[33] = E_X^{(3)}, & \mathcal{O}_X &\equiv \mathcal{O}_{\phi u}, \mathcal{O}_{\phi q}^{(3)}, \mathcal{O}_{\phi q}^{(1)}, & \alpha &= 1, 2 \\ \mathcal{C}_{\bar{X}}[ii] &= E_{\bar{X}}, & \mathcal{O}_{\bar{X}} &\equiv \mathcal{O}_{\phi e}, \mathcal{O}_{\phi d}, \mathcal{O}_{\phi l}^{(3)}, \mathcal{O}_{\phi l}^{(1)}, & i &= 1, 2, 3. \end{aligned}$$

Since for \mathcal{O}_{uW} and \mathcal{O}_{uB} only the $\mathcal{C}_{uW}[33]$ and $\mathcal{C}_{uB}[33]$ enter in our calculations, a total of 12 independent coefficients contribute to the EWPO at NLO, in agreement with Table 9 of [19].

The operators in Class B involving charge $\frac{2}{3}$ - quarks all have 4 u_R fields or 4 q_L fields. Retaining the contributions up to $\mathcal{O}(\frac{M_t^2}{v^2})$, the coefficients of \mathcal{O}_{uu} , $\mathcal{O}_{qq}^{(3)}$ and $\mathcal{O}_{qq}^{(1)}$ are subject to the following relations in the MFV scenario,

$$\begin{aligned} \text{Class B : } \mathcal{C}_Y[1122] &= \mathcal{C}_Y[2211] = A_Y, \mathcal{C}_Y[1221] = \mathcal{C}_Y[2112] = B_Y \\ \mathcal{C}_Y[33\alpha\alpha] &= \mathcal{C}_Y[\alpha\alpha 33] = A_Y^{(3)}, \mathcal{C}_Y[3\alpha\alpha 3] = \mathcal{C}_Y[\alpha 33\alpha] = B_Y^{(3)} \\ \mathcal{C}_Y[\alpha\alpha\alpha\alpha] &= A_Y + B_Y, \mathcal{C}_Y[3333] = 2(A_Y^{(3)} + B_Y^{(3)}) - A_Y - B_Y, \quad \alpha = 1, 2 \end{aligned} \quad (20)$$

which reduces the number of independent coefficients to 4 for each operator. The remaining operators in Class B satisfy the $U(3)^5$ relations of Eq. 17, thus resulting in 17 independent coefficients in Class B.

¹ We note that the (RR)(RR) operator, $\mathcal{O}_{ud}^{(8)}$, does not contribute to EWPOs at one-loop, and so our counting of the $U(1)^5$ operators agrees with Ref. [18].

² Since we assume that the CKM matrix is diagonal, there is no flavor violation in our implementation of the MFV scenario.

In Class C, the operators \mathcal{O}_{lu} , \mathcal{O}_{qe} , $\mathcal{O}_{qd}^{(1)}$, \mathcal{O}_{eu} , $\mathcal{O}_{ud}^{(1)}$, $\mathcal{O}_{lq}^{(1)}$, $\mathcal{O}_{lq}^{(3)}$ have 2 top quarks and they satisfy the relations:

$$\text{Class C : } \mathcal{C}_Z[\alpha\alpha ii] = D_Z, \mathcal{C}_Z[33ii] = D_Z^{(3)}, \quad \alpha = 1, 2, i = 1, 2, 3 \quad (21)$$

and hence we have 2 independent coefficients for each operator.

The only operator in Class C with 2 charge- $\frac{2}{3}$ quarks contributing to EWPOs is $\mathcal{O}_{qu}^{(1)}$ which satisfies the relations,

$$\begin{aligned} \text{Class C : } \mathcal{C}_{qu}^{(1)}[\alpha\alpha\beta\beta] &= D_{qu^{(1)}}, \mathcal{C}_{qu}^{(1)}[3333] = D_{qu^{(1)}}^{(33)} \\ \mathcal{C}_{qu}^{(1)}[33\alpha\alpha] &= D_{qu^{(1)}}^{(3)}, \mathcal{C}_{qu}^{(1)}[\alpha\alpha 33] = D_{qu^{(1)}}^{(3)}, \quad \alpha, \beta = 1, 2, \end{aligned} \quad (22)$$

and hence there are 4 independent flavor structures for $\mathcal{C}_{qu}^{(1)}$. The remaining operators in Class C, \mathcal{O}_{ed} , \mathcal{O}_{ld} and \mathcal{O}_{le} , satisfy the $U(3)^5$ relations and contribute 1 independent operator each. Overall, we have 21 independent coefficients in Class C. Excluding the operators $\mathcal{O}_{qd}^{(8)}$, $\mathcal{O}_{qu}^{(8)}$, and $\mathcal{O}_{ud}^{(8)}$ which do not contribute to EWPOs at NLO, our counting is in agreement with Table 2 of [20] and Table 9 of [19].

D. Flavor Assumptions: $U(2)^5$

Here we consider a scenario where the new physics distinguishes between the 3^{rd} generation and the first 2 generations. The first 2 generations are assumed to have the global symmetry[18],

$$G_2 \equiv U(2)_q \times U(2)_l \times U(2)_u \times U(2)_d \times U(2)_e. \quad (23)$$

Since we consider only the top quark mass to be non-zero, the $U(2)^5$ symmetry is unbroken.

Using the classification of operators given in Sec. II B, the G_2 symmetry requires that operators of Class A have the form:

$$\begin{aligned} \text{Class A : } \mathcal{C}_X[\alpha\alpha] &= E_X, \\ \mathcal{C}_X[33] &= E_X^{(3)}, \quad \alpha = 1, 2. \end{aligned} \quad (24)$$

There are 16 independent coefficients in this class.

The Class B operators satisfy

$$\begin{aligned} \text{Class B : } \mathcal{C}_Y[\alpha\alpha\beta\beta] &= A_Y, \mathcal{C}_Y[\alpha\beta\beta\alpha] = B_Y, \mathcal{C}_Y[\alpha\alpha\alpha\alpha] = A_Y + B_Y, \\ \mathcal{C}_Y[\alpha\alpha 33] &= \mathcal{C}_Y[33\alpha\alpha] = A_Y^{(3)}, \mathcal{C}_Y[3\alpha\alpha 3] = \mathcal{C}_Y[\alpha 33\alpha] = B_Y^{(3)}, \\ \mathcal{C}_Y[3333] &= F_Y^{(3)}, \quad \alpha \neq \beta, \alpha, \beta = 1, 2, \end{aligned} \quad (25)$$

so that each operator has 5 independent coefficients. As before, \mathcal{O}_{ee} has an extra constraint coming from the Fierz identities, which reduces the number of independent coefficients to 3 for this operator. Therefore, since $\mathcal{O}_{uu}[3333]$ does not contribute, Class B has 27 coefficients contributing to EWPOs at NLO in total.

The Class C operators, \mathcal{O}_C , contain 2 different fermion representations and the $U(2)^5$ symmetry implies,

$$\begin{aligned} \text{C : } \mathcal{C}_Z[\alpha\alpha\beta\beta] &= D_Z, \mathcal{C}_Z[3333] = D_Z^{(33)} \\ \mathcal{C}_Z[33\alpha\alpha] &= D_Z^{(3)}, \mathcal{C}_Z[\alpha\alpha 33] = D_Z^{(3)}, \quad \alpha, \beta = 1, 2, \end{aligned} \quad (26)$$

and there are 4 independent coefficients corresponding to each operator structure, for a total of 44 operators.

E. Third Generation Centric

In this scenario, only operators involving the 3rd generation fermions are non-zero. An example of such a scenario might be a Z' boson that only interacts with the 3rd generation. Operators of Class A in this scenario have the form:

$$\begin{aligned} \text{Class A : } \mathcal{C}_X[\alpha\alpha] &= 0, \\ \mathcal{C}_X[33] &= E_X^{(3)}, \quad \alpha = 1, 2. \end{aligned} \quad (27)$$

There are 9 real coefficients in this class.

The Class B and C operators satisfy

$$\begin{aligned} \text{Class B \& C : } \mathcal{C}_{Y,Z}[\alpha\alpha\beta\beta] &= \mathcal{C}_Y[\alpha\beta\beta\alpha] = 0, \\ \mathcal{C}_{Y,Z}[\alpha\alpha 33] &= \mathcal{C}_{Y,Z}[33\alpha\alpha] = \mathcal{C}_Y[3\alpha\alpha 3] = \mathcal{C}_Y[\alpha 33\alpha] = 0, \\ \mathcal{C}_Y[3333] &= F_Y^{(3)}, \mathcal{C}_Z[3333] = D_Z^{(3)}, \quad \alpha, \beta = 1, 2. \end{aligned} \quad (28)$$

For a total of 5 coefficients in Class B and 11 coefficients in Class C.

F. Third Generation Phobic

In this scenario, we assume that the new physics only couples to the 1st 2 generations. An example of such a model can be found in [42]. We assume no further symmetry, but note that the operators contributing to EWPOs do not have an arbitrary flavor structure, as described at the beginning of this section.

The flavor structure of the operators of Class A is

$$\begin{aligned} \text{Class A : } \mathcal{C}_X[\alpha\alpha] &= E_X^{(\alpha)}. \\ \mathcal{C}_X[33] &= 0, \quad \alpha = 1, 2, \end{aligned} \quad (29)$$

for a total of 14 independent coefficients.

For Class B we have

$$\begin{aligned} \text{Class B : } \mathcal{C}_Y[\alpha\alpha\alpha\alpha] &= F_Y^{(\alpha)}, \mathcal{C}_Y[\alpha\alpha\beta\beta] = A_Y^{(\alpha\beta)}, \mathcal{C}_Y[\alpha\beta\beta\alpha] = B_Y^{(\alpha\beta)}, \\ \mathcal{C}_Y[\alpha\alpha 33] &= \mathcal{C}_Y[33\alpha\alpha] = \mathcal{C}_Y[3\alpha\alpha 3] = \mathcal{C}_Y[\alpha 33\alpha] = \mathcal{C}_Y[3333] = 0, \quad \alpha \neq \beta, \alpha, \beta = 1, 2, \end{aligned} \quad (30)$$

corresponding to 4 independent coefficients for each operator (3 for \mathcal{O}_{ee}), for a total of 23 coefficients in Class B.

Finally for Class C the available structures are

$$\begin{aligned} \text{Class C : } \mathcal{C}_Z[\alpha\alpha\beta\beta] &= D_Z^{(\alpha\beta)} \\ \mathcal{C}_Z[\alpha\alpha 33] &= \mathcal{C}_Z[33\alpha\alpha] = \mathcal{C}_Z[3333] = 0, \quad \alpha, \beta = 1, 2, \end{aligned} \quad (31)$$

which again gives 4 independent coefficients for each operator, for a total of 44 coefficients in Class C.

G. Third Generation Phobic + $U(2)^5$

As a specific case of the previous example, we consider a scenario where, after assuming that new physics couples only to the 1st 2 generations, we further assume the existence of a $U(2)^5$ symmetry.

Operator	$U(3)^5$	MFV	$U(2)^5$	3^{rd} gen specific	3^{rd} gen phobic	3^{rd} gen phobic + $U(2)^5$	Flavorless
Class A	7	12	16	9	14	7	9
Class B	11	17	27	5	23	11	6
Class C	11	21	44	11	44	11	11
Total	29	50	87	25	81	29	26

Table II. Number of independent operators contributing to NLO predictions for EWPOs in various flavor scenarios.

In this case, the flavor structure of the operators of Class A is

$$\begin{aligned} \text{Class A : } \mathcal{C}_X[\alpha\alpha] &= E_X, \\ \mathcal{C}_X[33] &= 0, \quad \alpha = 1, 2, \end{aligned} \quad (32)$$

for a total of 7 independent coefficients.

For Class B we have

$$\begin{aligned} \text{Class B : } \mathcal{C}_Y[\alpha\alpha\beta\beta] &= A_Y, \quad \mathcal{C}_Y[\alpha\beta\beta\alpha] = B_Y, \quad \mathcal{C}_Y[\alpha\alpha\alpha\alpha] = A_Y + B_Y, \\ \mathcal{C}_Y[\alpha\alpha 33] &= \mathcal{C}_Y[33\alpha\alpha] = \mathcal{C}_Y[3\alpha\alpha 3] = \mathcal{C}_Y[\alpha 33\alpha] = \mathcal{C}_Y[3333] = 0, \quad \alpha \neq \beta, \alpha, \beta = 1, 2, \end{aligned} \quad (33)$$

corresponding to 2 independent coefficients for each operator (1 for \mathcal{O}_{ee}), for a total of 11 coefficients in Class B.

Finally for Class C the available structures are

$$\begin{aligned} \text{Class C : } \mathcal{C}_Z[\alpha\alpha\beta\beta] &= D_Z \\ \mathcal{C}_Z[\alpha\alpha 33] &= \mathcal{C}_Z[33\alpha\alpha] = \mathcal{C}_Z[3333] = 0, \quad \alpha, \beta = 1, 2, \end{aligned} \quad (34)$$

which again gives 1 independent coefficient for each operator, for a total of 11 coefficients in Class C.

H. Flavorless Scenario

This is the scenario employed in our previous calculations[33], where flavor plays no role and we simply drop all flavor indices. In this scenario, we assume that the operators have no flavor structure, that is we make the replacements,

$$\mathcal{C}_{X,Y,Z}[\dots] = A_{X,Y,Z}. \quad (35)$$

Therefore in this case there are 26 coefficients that contribute.

We summarize the results of our discussion of flavor scenarios in Table II. The number of operators contributing to EWPOs at NLO varies dramatically depending on the flavor structure and is significantly smaller than the 178 independent coefficients that contribute with no assumptions about flavor. We will see that these choices have large effects on the numerical results of fits to EWPOs.

III. NLO

This section describes our calculational procedure for the NLO corrections to the electroweak precision observables. Some of the results can be obtained from our previous calculation[33] by generalizing the flavor structure of each

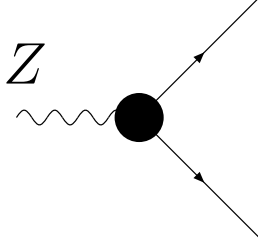


Figure 1. Z decays to fermions. The black circle represents the tree level SMEFT interaction.

observable. However, including a general flavor structure at NLO requires a new calculation for many of the flavor structures and observables. Therefore, we have performed the calculation in all generality and in this section we describe the details of the calculation and the assumptions that are implicit in the numerical results of the next section.

At tree level, the interactions are just the Z (and W) decays to 2 fermions shown in Fig. 1 and the effect of including the dimension-6 SMEFT contributions is to change the vector boson couplings to fermions. The tree level SMEFT couplings of fermions to the Z and W are given in terms of our input parameters (α, M_Z, G_μ) ,

$$\begin{aligned}
L \equiv & 2M_Z \sqrt{\sqrt{2}G_\mu} \left\{ Z_\mu \left[g_L^{Zq} + \delta g_L^{Zq} \right] \bar{q} \gamma_\mu q + Z_\mu \left[g_R^{Zu} + \delta g_R^{Zu} \right] \bar{u}_R \gamma_\mu u_R \right. \\
& + Z_\mu \left[g_R^{Zd} + \delta g_R^{Zd} \right] \bar{d}_R \gamma_\mu d_R + Z_\mu \left[g_L^{Zl} + \delta g_L^{Zl} \right] \bar{l} \gamma_\mu l \\
& \left. + Z_\mu \left[g_R^{Ze} + \delta g_R^{Ze} \right] \bar{e}_R \gamma_\mu e_R + Z_\mu \left(\delta g_R^{Z\nu} \right) \bar{\nu}_R \gamma_\mu \nu_R \right\} \\
& + 2M_W [\alpha, M_Z, G_\mu] \sqrt{\frac{G_\mu}{\sqrt{2}}} \left\{ W_\mu \left[(1 + \delta g_L^{Wq}) \bar{u}_L \gamma_\mu d_L + \left(\delta g_R^{Wq} \right) \bar{u}_R \gamma_\mu d_R \right] \right. \\
& \left. + W_\mu \left[(1 + \delta g_L^{Wl}) \bar{\nu}_L \gamma_\mu e_L + \left(\delta g_R^{W\nu} \right) \bar{\nu}_R \gamma_\mu e_R \right] + h.c. \right\}, \tag{36}
\end{aligned}$$

where at tree level,

$$\begin{aligned}
g_R^{Zf} &= -s_W^2 Q_f \quad \text{and} \quad g_L^{Zf} = T_3^f - s_W^2 Q_f \\
s_W^2 &\equiv 1 - \frac{M_W^2[\alpha, M_Z, G_\mu]}{M_Z^2}, \tag{37}
\end{aligned}$$

$T_3^f = \pm \frac{1}{2}$, and $M_W^2[\alpha, M_Z, G_\mu]$ is the mass of the W boson written in terms of the (α, M_Z, G_μ) input parameters as defined later in Sec. III D. Analytic expressions for the shifts in the couplings in terms of the Warsaw basis coefficients can be found in [43, 44].

We use the SMEFT Feynman rules of Ref. [2] as implemented in FeynRules [45] from which a FeynArts [46] model file is obtained. In this way, we are able to generate the relevant one-loop and real emission amplitudes, which include all the QCD and EW corrections to the Z and W pole observables considered here. All the amplitudes are generated in R_ξ gauge, and the gauge invariance of the final results is verified explicitly. The results of the previous step are manipulated with FeynCalc [47, 48], which is also used to reduce the integrals that appear in terms of Passarino-Veltman integrals [49]. We retain only terms of $\mathcal{O}(v^2/\Lambda^2)$, since the SMEFT is renormalizable at fixed order in the

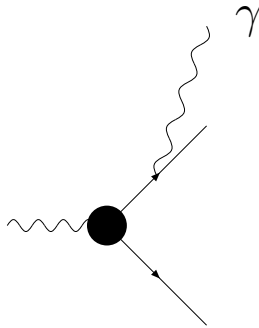


Figure 2. Z decays to 2 fermions, including real photon emission. The black circle represents the tree level SMEFT interaction.

(v^2/Λ^2) expansion³. As is the case of the pure SM results, the Feynman diagrams that contribute to the calculations are afflicted by both UV and IR divergences and we describe the regulation of these singularities below.

A. Real contributions

The decays of the Z and W bosons receive contributions from real photon and gluon emissions (as demonstrated generically in Fig. 2), which are necessary to cancel the IR divergences from the virtual contributions. From Fig. 2, it is clear that the flavor structure of the real emission diagrams is identical to that of the tree level result. Due to the complicated tensor structures of the SMEFT vertices, it is convenient to avoid integration over the final state 3-body phase space and therefore we use the method of Ref. [50], replacing the integration over the phase space with a loop integration. Specifically, we square the tree-level real amplitudes and then make use of the identity,

$$2i\pi\delta(p^2 - m^2) = \frac{1}{p^2 - m^2 + i0} - \frac{1}{p^2 - m^2 - i0}, \quad (38)$$

to build a correspondence between phase space integrals and the imaginary part of 2-loop integrals, which we calculate by rewriting them in terms of known master integrals [51, 52] using FIRE [53]. We notice that only the imaginary parts that correspond to a cut through all three particles in the final state contribute to the phase space integral, and thus particular attention has to be taken in isolating the correct imaginary part. We then check that the results obtained with this technique reproduce the known results for the real photon and gluon contributions to the SM NLO results. Finally, we treat IR divergences in the real and virtual contributions by giving a small mass to photons and gluons, and then carefully taking the massless limit of the full result[54].

B. Virtual contributions

At LO, the amplitudes can be written in terms of the EW vacuum expectation value (v), the pole masses of the Z and W bosons, and the Wilson coefficients of SMEFT operators in Table I. Tree level results for the observables of Eq. 5 are given in Appendix A of [33]. This reference also includes the NLO results in the case where the 2-fermion and 4-fermion operators are assumed to be independent of flavor. The virtual diagrams consist of the full set of one-loop EW and QCD diagrams with the SMEFT vertices. Contributions of special interest to the study of the flavor structure arise from the 4-fermion interactions shown in Fig. 3. In what follows, we do not assume any flavor structure for the 4 fermion operators, although as noted in Sec. II, only certain flavor structures arise.

³ Including terms resulting from squaring the LO EFT result would result in contributions of $\mathcal{O}(v^4/\Lambda^4)$, which is the same order as the dimension-8 terms we are neglecting, and hence would be inconsistent.

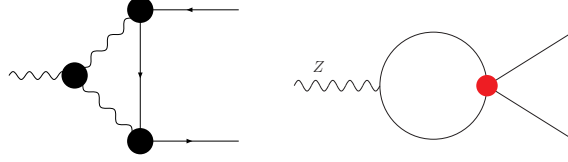


Figure 3. Sample virtual one-loop contributions to Z decays to 2 fermions. The black circles represent SMEFT insertions correcting the SM vertices, while the red circle denotes the dimension-6 4-fermion operators.

C. UV counterterms

To treat the UV divergences we use dimensional regularization in d dimensions so that the poles are written in terms of the regulator $\epsilon = (4 - d)/2$, which are later canceled by adding appropriate counterterms.

Note that we chose to exactly cancel all the tadpole contributions, that is we put to zero from the beginning all the diagrams that contain tadpoles. This corresponds to identifying the renormalized vacuum with the (gauge-dependent) minimum of the renormalized Higgs potential[55]. Consequently, all intermediate quantities are in general gauge dependent and only the final physical observables are gauge independent. Therefore, the cancellation of the R_ξ gauge parameter is highly non trivial and a strong check of the correctness of the calculation.

Since we do not have direct measurements of the coefficients of the dimension-6 operators, we treat them as \overline{MS} parameters by constructing renormalized coefficients, $\mathcal{C}_i(\mu)$, of the form

$$\mathcal{C}_i(\mu) = \mathcal{C}_{0,i} + \delta\mathcal{C}_i = \mathcal{C}_{0,i} - \frac{1}{2\hat{\epsilon}} \frac{1}{16\pi^2} \gamma_{ij} \mathcal{C}_j, \quad (39)$$

where we define $\hat{\epsilon}^{-1} \equiv \epsilon^{-1} - \gamma_E + \log(4\pi)$. In the previous equation, μ is the renormalization scale, $\mathcal{C}_{0,i}$ are the bare quantities, and γ_{ij} are the one-loop anomalous dimensions defined by the relation

$$\mu \frac{d\mathcal{C}_i}{d\mu} = \frac{1}{16\pi^2} \gamma_{ij} \mathcal{C}_j. \quad (40)$$

The complete set of anomalous dimensions for dimension-6 SMEFT operators in the Warsaw basis is in Refs. [23–25]. In general the γ_{ij} are not diagonal and 4-fermion operators mix with 2-fermion and other operators under renormalization.

Regarding the SM input parameters, we use the on-shell (OS) scheme which defines the renormalized quantities in terms of measured observables, and specifically we choose $\{\alpha, G_\mu, M_Z\}$ as the independent inputs[44, 56].

The vacuum expectation value v is connected to the Fermi constant G_μ by the relation,

$$G_\mu + \frac{1}{\sqrt{2}\Lambda^2} \mathcal{C}_U[1221] - \frac{1}{\sqrt{2}\Lambda^2} (\mathcal{C}_{\phi l}^{(3)}[11] + \mathcal{C}_{\phi l}^{(3)}[22]) \equiv \frac{1}{\sqrt{2}v_0^2} (1 + \Delta r), \quad (41)$$

where the \mathcal{C} in Eq. 41 are the renormalized $\mathcal{C}_i(\mu)$, v_0 is the unrenormalized minimum of the potential (where we use the notation '0' to denote the tree level relation), and Δr is extracted from the calculation of muon decay at 1-loop at zero momentum transfer. The result for Δr in terms of the dimension-6 coefficients is in Appendix D of [26].

For the mass of the Z boson, the relation between the bare and renormalized quantity is obtained from the formula

$$M_Z^2 = M_{0,Z}^2 - \Pi_{ZZ}(M_Z^2), \quad (42)$$

where $M_{0,Z}^2$ is the bare quantity and $\Pi_{ZZ}(M_Z^2)$ is the one-loop correction to the 2-point function for Z, which is reported analytically for the SMEFT in Refs. [57, 58]. It is also convenient to define the one-loop corrections to the W boson 2-point function $\Pi_{WW}(M_W^2)$ in a similar manner.

The relation between the bare and renormalized electromagnetic coupling α is

$$\alpha(M_Z) = \frac{\alpha}{1 - \Delta\alpha(M_Z)}, \quad (43)$$

where we derive $\Delta\alpha$ from the 1-loop SMEFT corrections to the $\gamma\bar{e}e$ vertex. Note that $\Delta\alpha$ receives non-perturbative corrections from diagrams involving light quarks that contribute to the vacuum polarization $\Pi_{\gamma\gamma}^{(5)}(0)$. To treat these contributions we use the hadronic contribution to $\Delta\alpha$ which is defined as

$$\Delta\alpha_{\text{had}}^{(5)}(M_Z) = 4\pi\alpha \left(\Pi_{\gamma\gamma}^{(5)}(M_Z) - \Pi_{\gamma\gamma}^{(5)}(0) \right), \quad (44)$$

where $\Pi_{\gamma\gamma}^{(5)}(M_Z)$ is a perturbative correction obtained by calculating the same diagrams that contribute to $\Pi_{\gamma\gamma}^{(5)}(0)$. The value of the hadronic contribution to $\Delta\alpha$ is obtained using dispersion relations and experimental data and we report it in Eq. 59 together with other inputs.

Finally, it is convenient to define the quantities

$$\Delta\rho \equiv \Pi_{WW}(M_W^2)/M_W^2 - \Pi_{ZZ}(M_Z^2)/M_Z^2 \quad \text{and} \quad (45)$$

$$\Delta r_W \equiv \Delta r + \Pi_{WW}(M_W^2)/M_W^2, \quad (46)$$

which will enter in some of the definitions in the following section.

D. M_W calculation

The relation between the mass of the W boson and the input parameters in the SM is given by the well-known formula

$$M_{W,SM}^2 = M_Z^2 \left(1 + \sqrt{1 - \frac{4\pi\alpha(1 + \Delta\bar{r}_{SM})}{\sqrt{2}M_Z^2 G_\mu}} \right), \quad (47)$$

where we use a slightly unusual notation to distinguish between the finite gauge-invariant $\Delta\bar{r}$ and the UV divergent gauge-dependent Δr . $\Delta\bar{r}_{SM}$ is obtained from the previous corrections:

$$\Delta\bar{r}_{SM} = \Delta\alpha_{SM} - \frac{\cos^2\theta_W}{\sin^2\theta_W} \Delta\rho_{SM} + \Delta r_{W,SM}, \quad (48)$$

where θ_W is the weak mixing angle, which is defined in the OS scheme as $\cos\theta_W \equiv M_W/M_Z$.

In the SMEFT, Eq. 47 is modified:

$$M_W^2 = M_Z^2 \left(1 + \sqrt{1 - \frac{4\pi\alpha(1 + \Delta\bar{r})}{\sqrt{2}M_Z^2 G_\mu}} - \frac{1}{16} \frac{1}{\sqrt{2}G_\mu\Lambda^2} \left(\frac{\cos\theta_W}{\cos 2\theta_W} \right)^3 (F_1 G_1 + F_2 G_2) \right), \quad (49)$$

where

$$\begin{aligned} \Delta\bar{r} = & \Delta\alpha - \frac{\cos^2\theta_W}{\sin^2\theta_W} \Delta\rho + \Delta r_W \\ & + \frac{1}{\sqrt{2}G_\mu\Lambda^2} \left(-\frac{\cos\theta_W(\cos\theta_W C_{\phi D} + 2\sin\theta_W C_{\phi WB})}{2\sin^4\theta_W} \Delta\rho_{SM} \right. \\ & + \frac{\cos\theta_W(\cos\theta_W C_{\phi D} + 4\sin\theta_W C_{\phi WB})}{2\sin^2\theta_W} \left(\Delta r_{W,SM} - \frac{\Pi_{WW,SM}(M_W^2)}{M_W^2} \right) \\ & \left. + \frac{\cos^2\theta_W}{2\sin^2\theta_W} \delta\mathcal{C}_{\phi D} + \frac{2\cos\theta_W}{\sin\theta_W} \delta\mathcal{C}_{\phi WB} \right), \end{aligned} \quad (50)$$

and we define

$$G_1 = \cos\theta_W C_{\phi D} + 4\sin\theta_W C_{\phi WB} + \sin\theta_W \tan\theta_W (2C_{\phi l}^{(3)}[11] + 2C_{\phi l}^{(3)}[22] - 2C_{ll}[1221]) \quad (51)$$

$$G_2 = \cos\theta_W C_{\phi D} + 2\sin\theta_W C_{\phi WB} \quad (52)$$

$$F_1 = 4 + 6\Delta r_{SM} + 2(2 + \Delta r_{SM}) \cos 4\theta_W - M_Z^2 \frac{\partial \Delta r_{SM}}{\partial (M_W^2)} \sin 2\theta_W \sin 4\theta_W \quad (53)$$

$$F_2 = -8\Delta r_{SM} \cos 2\theta_W. \quad (54)$$

It is convenient to rewrite Eq. 49 as,

$$M_W^2 = M_{W,SM}^2 + \frac{1}{\sqrt{2}G_\mu\Lambda^2} M_{W,EFT}^2 \quad (55)$$

where $M_{W,SM}^2$ is obtained from Eq. 47, and we separate the SM and EFT contributions. At NLO, the mass of the W boson is

$$M_{W,NLO} = \sqrt{M_{W,SM}^2 + \frac{1}{\sqrt{2}G_\mu\Lambda^2} M_{W,EFT}^2} \approx \sqrt{M_{W,SM}^2} + \frac{1}{\sqrt{2}G_\mu\Lambda^2} \frac{M_{W,EFT}^2}{2\sqrt{M_{W,SM}^2}}, \quad (56)$$

and we calculate $M_{W,SM}^2$ and $M_{W,EFT}^2$ at 1-loop. Note that the calculation of $M_{W,SM}^2$ and $M_{W,EFT}^2$ involve the mass of the W itself that enters through $\cos\theta_W$. In this case, we use the value of M_W obtained from Eq. 47 after putting $\Delta\bar{r} \rightarrow 0$. As the last step in our calculation, we replace the SM result from our calculation with the "best" theory result of Table III, obtaining our final expression for the mass of the W boson:

$$M_{W,fin} = M_{W,"best"} + \frac{1}{\sqrt{2}G_\mu\Lambda^2} \frac{M_{W,EFT}^2}{2\sqrt{M_{W,SM}^2}}. \quad (57)$$

All the other observables that we include in our fit depend on the mass of the W boson in some way. In our numerical calculation of a generic observable, O , we use our best knowledge of M_W (Eq. 57) in the calculation of the LO contributions to O and $M_{W,NLO}$ in Eq. 56 in the calculation of the NLO contributions to O . Afterwards, we replace our SM result with the "best" theory results in table III. Finally, our EWPOs are expressed as

$$O = O_{"best"} + O_{EFT,LO}|_{M_W \rightarrow M_{W,fin}} + O_{EFT,NLO}|_{M_W \rightarrow M_{W,NLO}}. \quad (58)$$

We close this section with a few remarks about the validity of our expansion. After renormalization, the amplitude is finite. We then square the amplitude and retain only terms that are linear in the SMEFT coefficients. In principle, we could retain the terms quadratic in the SMEFT coefficients as this is also finite. However, the quadratic contributions generically have the same counting in factors of $\frac{1}{16\pi^2}$ as does a 2-loop SMEFT contribution with 2 insertions of SMEFT coefficients interfering with the SM amplitude. Furthermore, the quadratic terms contain contributions from SMEFT operators that we have dropped because they don't interfere with the SM.⁴

IV. RESULTS

In this section, we show the effects of the flavor assumptions on global fits to EWPOs. We fit to the data given in Table III and we use the Particle Data Group review[59] value for M_W . The column labelled "best" theory corresponds to predictions computed to the highest available order in perturbation theory. We take as our input parameters,

$$\begin{aligned} G_\mu &= 1.1663787(6) \times 10^{-5} \text{GeV}^{-2} \\ M_Z &= 91.1876 \pm .0021 \text{GeV} \\ \frac{1}{\alpha} &= 137.035999139(31) \\ \Delta\alpha_{\text{had}}^{(5)} &= 0.02768 \pm 0.00009 \\ \alpha_s(M_Z) &= 0.1181 \pm 0.0011 \\ M_h &= 125.25 \pm 0.17 \text{ GeV} \\ M_t &= 172.69 \pm 0.5 \text{ GeV}. \end{aligned}$$

⁴ The quadratic contributions corresponding to the square of the amplitude computed here can be obtained from the authors on request.

The SMEFT scale is always taken to be $\Lambda = 1$ TeV and the coefficient functions are evaluated at the renormalization scale $\mu = M_Z$.

Flavor blind predictions for EWPOs were presented in Ref. [35], which corresponds to the scenario labeled flavorless here.⁵ In this section, we concentrate on the derivation of limits on SMEFT coefficients that are dependent on the assumed flavor scenario. Our limits are obtained by considering only one non-zero operator type, $\mathcal{O}[ijkl]$, at a time and imposing the flavor symmetries described in Sec. II. The single parameter limits are marginalized over the other independent flavor structures. Before proceeding, we find it convenient to briefly describe the marginalization procedure we use to obtain our results. Assuming Gaussian uncertainties, we calculate the χ^2 function

$$\chi^2(\mathcal{C}) = \sum_{i,j} (O_i^{\text{exp}} - O_i^{\text{th}}) \sigma_{ij}^{-2} (O_j^{\text{exp}} - O_j^{\text{th}}), \quad (59)$$

where O_i^{exp} and O_i^{th} are the experimental and theoretical values of a certain observable O_i respectively and σ_{ij}^2 is the covariance matrix. In general, we can write $\chi^2(\mathcal{C}) \equiv \chi^2(\bar{\mathcal{C}}, \hat{\mathcal{C}})$ as a function of coefficients $\bar{\mathcal{C}}$, which we are interested in finding the limits of, and coefficients $\hat{\mathcal{C}}$, which we want to marginalize over. As a first step, we find the values of $\hat{\mathcal{C}}$ that minimize χ^2 while keeping $\bar{\mathcal{C}}$ free. In other words, we find the $\hat{\mathcal{C}}_M(\bar{\mathcal{C}})$ that satisfy the system of equations

$$\left. \frac{\partial \chi^2}{\partial \hat{\mathcal{C}}} \right|_{\hat{\mathcal{C}} = \hat{\mathcal{C}}_M(\bar{\mathcal{C}})} = 0, \quad (60)$$

where we highlighted that the $\hat{\mathcal{C}}_M$ are defined as function of the free parameters $\bar{\mathcal{C}}$. We can now define,

$$\chi^2(\bar{\mathcal{C}}) \equiv \chi^2(\bar{\mathcal{C}}, \hat{\mathcal{C}} = \hat{\mathcal{C}}_M). \quad (61)$$

The new function $\chi^2(\bar{\mathcal{C}})$ is used to perform the necessary studies. More details on this procedure can be found in the literature (see for example [14, 60, 61]).

For example, we can study the χ^2 for the coefficient $C_{qq}^{(1)}$ in the MFV scenario. The χ^2 function is given by:

$$\begin{aligned} \chi_{\text{MFV}}^2 \left(C_{qq}^{(1)} \right) = & 21.0184 - 0.183188 C_{qq}^{(1)}[1, 1, 2, 2] + 0.00528431 C_{qq}^{(1)}[1, 1, 2, 2]^2 - 0.193834 C_{qq}^{(1)}[1, 1, 3, 3] \\ & + 0.00725802 C_{qq}^{(1)}[1, 1, 2, 2] C_{qq}^{(1)}[1, 1, 3, 3] + 0.120819 C_{qq}^{(1)}[1, 1, 3, 3]^2 + 5.33703 C_{qq}^{(1)}[1, 3, 3, 1] \\ & - 0.2973 C_{qq}^{(1)}[1, 1, 2, 2] C_{qq}^{(1)}[1, 3, 3, 1] - 0.271204 C_{qq}^{(1)}[1, 1, 3, 3] C_{qq}^{(1)}[1, 3, 3, 1] + 4.19859 C_{qq}^{(1)}[1, 3, 3, 1]^2 \\ & - 5.92823 C_{qq}^{(1)}[3, 3, 3, 3] + 0.163898 C_{qq}^{(1)}[1, 1, 2, 2] C_{qq}^{(1)}[3, 3, 3, 3] + 0.0186148 C_{qq}^{(1)}[1, 1, 3, 3] C_{qq}^{(1)}[3, 3, 3, 3] \\ & - 4.83774 C_{qq}^{(1)}[1, 3, 3, 1] C_{qq}^{(1)}[3, 3, 3, 3] + 3.85299 C_{qq}^{(1)}[3, 3, 3, 3]^2. \end{aligned} \quad (62)$$

Following the above procedure, to marginalize $C_{qq}^{(1)}[1, 1, 2, 2]$ and $C_{qq}^{(1)}[3, 3, 3, 3]$, we have

$$\begin{cases} \frac{\partial \chi_{\text{MFV}}^2}{\partial C_{qq}^{(1)}[1, 1, 2, 2]} = 0 \\ \frac{\partial \chi_{\text{MFV}}^2}{\partial C_{qq}^{(1)}[3, 3, 3, 3]} = 0 \end{cases} \implies \begin{cases} C_{qq}^{(1)}[1, 1, 2, 2] \rightarrow 8.062020 - 0.9688560 C_{qq}^{(1)}[1, 1, 3, 3] + 27.44810 C_{qq}^{(1)}[1, 3, 3, 1] \\ C_{qq}^{(1)}[3, 3, 3, 3] \rightarrow 0.597832 + 0.0181909 C_{qq}^{(1)}[1, 1, 3, 3] + 0.0439991 C_{qq}^{(1)}[1, 3, 3, 1] \end{cases}. \quad (63)$$

Setting the marginalized coefficients to their minimum we find:

$$\begin{aligned} \chi_{\text{MFV}}^2 \left(C_{qq}^{(1)}[1, 1, 3, 3], C_{qq}^{(1)}[1, 3, 3, 1] \right) = & 18.5079 - 0.124191 C_{qq}^{(1)}[1, 1, 3, 3] + 0.117473 C_{qq}^{(1)}[1, 1, 3, 3]^2 + 0.048042 C_{qq}^{(1)}[1, 3, 3, 1] \\ & - 0.0711661 C_{qq}^{(1)}[1, 1, 3, 3] C_{qq}^{(1)}[1, 3, 3, 1] + 0.012012 C_{qq}^{(1)}[1, 3, 3, 1]^2. \end{aligned} \quad (64)$$

The new χ^2 , that now depends only on $C_{qq}^{(1)}[1, 1, 3, 3]$ and $C_{qq}^{(1)}[1, 3, 3, 1]$, is used to carry out the required analysis for the MFV scenario.

⁵ The exact numerical results of this work differ slightly from Ref. [35] since we fit to an expanded set of measurements with slightly different numerical values for the inputs.

Measurement	Experiment	"Best" theory
$\Gamma_Z(\text{GeV})$	2.4955 ± 0.0023	2.4943 ± 0.0006 [62–64]
R_e	20.804 ± 0.05	20.732 ± 0.009 [62–64]
R_μ	20.784 ± 0.034	20.732 ± 0.009 [62–64]
R_τ	20.764 ± 0.045	20.779 ± 0.009 [62–64]
R_b	0.21629 ± 0.00066	0.2159 ± 0.0001 [62–64]
R_c	0.1721 ± 0.0030	0.1722 ± 0.00005 [62–64]
σ_h	41.481 ± 0.033	41.492 ± 0.008 [62–64]
$A_e(\text{from } A_{LR} \text{ had})$	0.15138 ± 0.00216	0.1469 ± 0.0004 [64, 65]
$A_e(\text{from } A_{LR} \text{ lep})$	0.1544 ± 0.0060	0.1469 ± 0.0004 [64, 65]
$A_e(\text{from Bhabba pol})$	0.1498 ± 0.0049	0.1469 ± 0.0004 [64, 65]
A_μ	0.142 ± 0.015	0.1469 ± 0.0004 [64, 65]
$A_\tau(\text{from SLD})$	0.136 ± 0.015	0.1469 ± 0.0004 [64, 65]
$A_\tau(\tau \text{ pol})$	0.1439 ± 0.0043	0.1469 ± 0.0004 [64, 65]
A_c	0.670 ± 0.027	0.66773 ± 0.0002 [64, 65]
A_b	0.923 ± 0.020	0.92694 ± 0.00006 [64–66]
A_s	0.895 ± 0.091	0.93563 ± 0.00004 [64, 65]
$A_{e,FB}$	0.0145 ± 0.0025	0.0162 ± 0.0001 [64, 65]
$A_{\mu,FB}$	0.0169 ± 0.0013	0.0162 ± 0.0001 [64, 65]
$A_{\tau,FB}$	0.0188 ± 0.0017	0.0162 ± 0.0001 [64, 65]
$A_{b,FB}$	0.0996 ± 0.0016	0.1021 ± 0.0003 [64–66]
$A_{c,FB}$	0.0707 ± 0.0035	0.0736 ± 0.0003 [64, 65]
$A_{s,FB}$	0.0976 ± 0.0114	0.10308 ± 0.0003 [64, 65]
$M_W(\text{GeV})$ PDG World Ave	80.377 ± 0.012	80.357 ± 0.006 [67, 68]
$\Gamma_W(\text{GeV})$	2.085 ± 0.042	2.0903 ± 0.0003 [69]

Table III. Unless otherwise cited, experimental results are taken from Table 10.5 of the Particle Data Group[59]. The theory results include the full set of 2-loop contributions for the Z pole observables, along with higher order corrections when known. The theory predictions are computed using the formulae in the indicated references and our input parameters, and the theory errors include the parametric uncertainties on M_t and M_h [64], along with the estimated theory uncertainties described in the respective papers.

We begin by considering limits on the 2-fermion operators (Class A) that contribute to the Z and W boson observables listed in Eq. 5. Table IV compares the LO and NLO results for the SMEFT coefficients in the $U(3)^5$, MFV, and 3^{rd} generation centric scenarios. We note that the $U(3)^5$ and flavorless scenarios are identical for the coefficients of the 2-fermion operators. The limits on flavor structures that are not listed in the table can be derived using the results of Section II, although for clarity we list limits on some of the non-independent coefficients. The differences between the LO and NLO fits are in general quite small. The single parameter limits are compared graphically in Fig. 4 where we see differences up to factors of 2 between the various flavor assumptions.

The contributions of top quark loops to the 2-fermion operators have been studied in [70]. Table 3 of this reference presents the 95% CL single parameter limits on C_{uW} [33], C_{uB} [33], $C_{\phi u}$ [33] and $C_{\phi q}^{(-)}$ [33] $\equiv \frac{1}{2}(C_{\phi q}^{(1)}[33] - C_{\phi q}^{(3)}[33])$. Our results agree with these to $\sim 10 - 20\%$, which is consistent with the use of slightly different sets of data as input.

In Fig. 5 and in Figs. 12-17 in the appendix, we show on the left hand side the limits on the 2-fermion operators in the $U(3)^5$, 3^{rd} generation specific, and MFV scenarios. On the right hand side of these plots we show the 3^{rd} generation phobic and 3^{rd} generation phobic + $U(2)^5$ scenarios, where the new physics only couples to the first and second generations, and the flavorless scenario. It is apparent that the limits one quotes on these operators is highly dependent on the assumed flavor scenario. It is interesting to note in Fig. 5, the large differences in the shapes of the LO and NLO fits in the MFV and 3^{rd} generation phobic scenarios and that the limits on the 3^{rd} generation phobic scenario are considerably weaker than in the other scenarios.

Tables V and VI show the 95% CL limits on coefficients in the flavor schemes discussed in Sec. II for the Class B and Class C operators. In general, there is a strong dependence on the flavor scenario. This dependence is much larger than for the 2-fermion operator coefficients and the flavorless scenario gives much more stringent bounds for many

95 % CL limits on 2-fermion operators from EWPOs

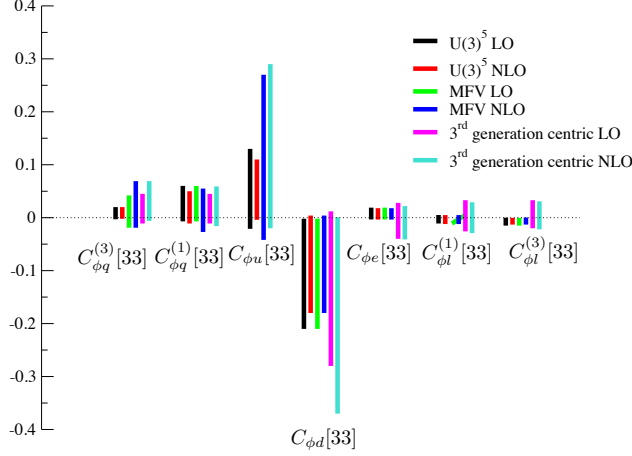


Figure 4. Limits on coefficients of 2-fermion operators in the $U(3)^5$ (LO in black, NLO in red), MFV (LO in green, NLO in blue) and 3^{rd} generation centric (LO in magenta, NLO in cyan) scenarios with a single non-zero operator and marginalizing over the other independent flavor structures of each operator.

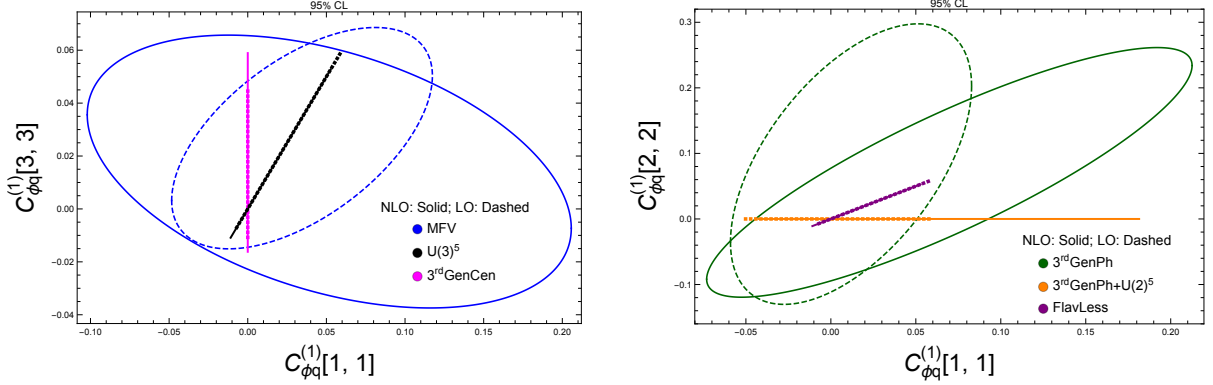


Figure 5. 95% CL limits on $\mathcal{C}_{\phi q}^{(1)}[ij]$ under flavor assumptions described in the text. Results at LO are drawn with dashed lines, results at NLO are drawn with solid lines. **On the left** we present $\mathcal{C}_{\phi q}^{(1)}[11]$ vs. $\mathcal{C}_{\phi q}^{(1)}[33]$ in the $U(3)^5$ (black), MFV (blue) and 3^{rd} generation centric (magenta) scenarios. In these scenarios $\mathcal{C}_{\phi q}^{(1)}[22] = \mathcal{C}_{\phi q}^{(1)}[11]$. **On the right** we present $\mathcal{C}_{\phi q}^{(1)}[11]$ vs. $\mathcal{C}_{\phi q}^{(1)}[22]$ in the 3^{rd} generation phobic (green), 3^{rd} generation phobic + $U(2)^5$ (orange) and flavorless (violet) scenarios. In the first two scenarios $\mathcal{C}_{\phi q}^{(1)}[33] = 0$, while in the flavorless scenario $\mathcal{C}_{\phi q}^{(1)}[33] = \mathcal{C}_{\phi q}^{(1)}[22] = \mathcal{C}_{\phi q}^{(1)}[11]$. All other coefficients are set to 0.

coefficient functions than is the case in the other flavor scenarios.

The most precise limits are on \mathcal{C}_U and are shown in Fig. 6 for several flavor scenarios. It is clear that using the flavorless scenario gives limits that are factors of $\mathcal{O}(10 - 100)$ more precise than in the MFV or $U(3)^5$ scenarios for \mathcal{C}_U . This is understood from Eq. 6 where we see that the only flavor structure that contributes to G_μ is $\mathcal{C}_U[1221]$ and we observe that the limits on \mathcal{C}_U in the $U(2)^5$ scenario are the weakest. In Fig. 7, we show the strong correlation between $\mathcal{C}_U[1221]$ and $\mathcal{C}_U[3333]$ in the MFV scenario and between $\mathcal{C}_U[1221]$ and $\mathcal{C}_U[1122]$ in the $U(2)^5$ and 3^{rd} generation phobic scenarios. We note that there are only 2 independent \mathcal{C}_U coefficients.

Marginalized single parameter limits on the Class B operator coefficients $\mathcal{C}_{qq}^{(1)}$ and $\mathcal{C}_{qq}^{(3)}$ are shown in Fig. 8. The $U(3)^5$ and MFV results for these operators are within a factor of 2 of each other, while the 3^{rd} generation specific and 3^{rd} generation phobic scenarios are weakly constrained. Sample correlations between different flavor structures are shown

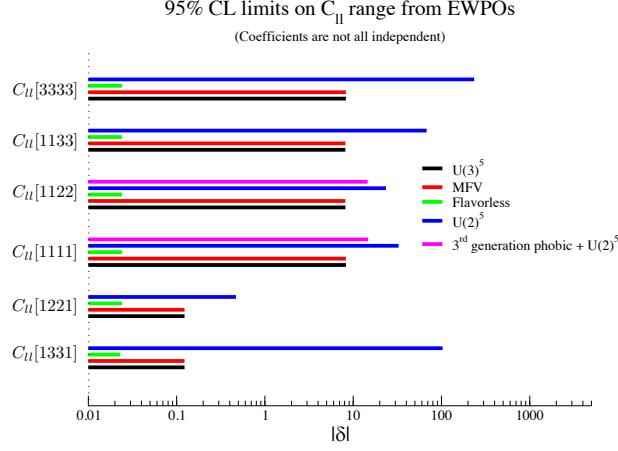


Figure 6. Limits on coefficients of $C_U[ijkl]$ in various flavor scenarios, where $i, j, k, l = 1, 2, 3$. Only C_{II} is taken to be non-zero in this figure, and the independent flavor structures not shown are marginalized over. Exact numbers are given in Table V.

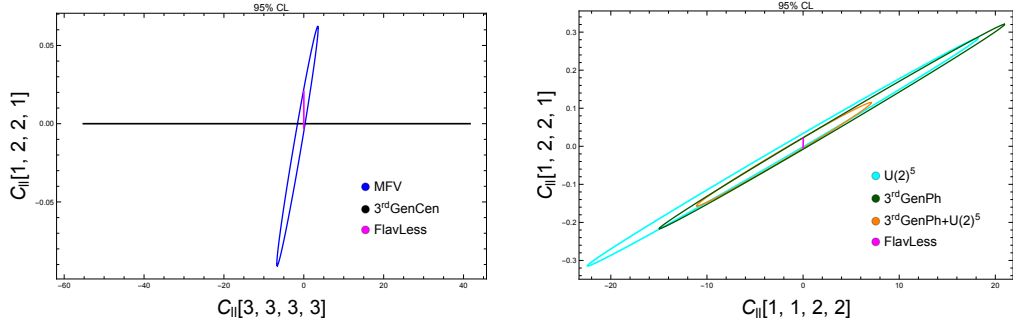


Figure 7. 95% CL limits on C_{II} in various flavor scenarios with all other coefficients taken to be 0. **On the left** we present $C_{II}[3333]$ vs. $C_{II}[1221]$ in the MFV (blue), 3^{rd} generation centric (black) and flavorless (magenta) scenarios. **On the right** we present $C_{II}[1122]$ vs. $C_{II}[1221]$ in the $U(2)^5$ (cyan), 3^{rd} generation phobic (green), 3^{rd} generation phobic + $U(2)^5$ (orange) and flavorless (magenta) scenarios. All the independent flavor structures not present in the plots are marginalized over.

in Fig. 9, demonstrating the sensitivity to the flavor assumptions of these fits.

The 4-fermion Class C operators can be studied individually, and marginalizing over the independent flavor structures gives the limits in Fig. 10. The limits obtained in the flavorless setup in this case also similar to those of the MFV and $U(3)^5$ flavor structures. The 3^{rd} generation specific and 3^{rd} generation phobic scenarios give weak bounds for these operators. In addition, there are large correlations between the different flavor structures, as illustrated in Fig. 11.

V. CONCLUSIONS

Measurements at the Z and W boson poles provide important limits on BSM physics. Using tree level predictions, the fermion-gauge boson interactions are restricted to be quite close to those of the SM. In the context of the SMEFT, the bounds on anomalous particle couplings can be extended to systematically include NLO QCD and EW effects and interpreted as bounds on dimension-6 SMEFT operators. These bounds were previously derived ignoring the effects of the flavor dependence of the dimension-6 2- and 4-fermion operators. We have re-computed the NLO contributions to EWPOs including an arbitrary flavor structure for the fermion operators. With the exception of C_{II} (which contributes to muon decay and is quite precisely bounded), the operators that contribute to EWPOs at tree

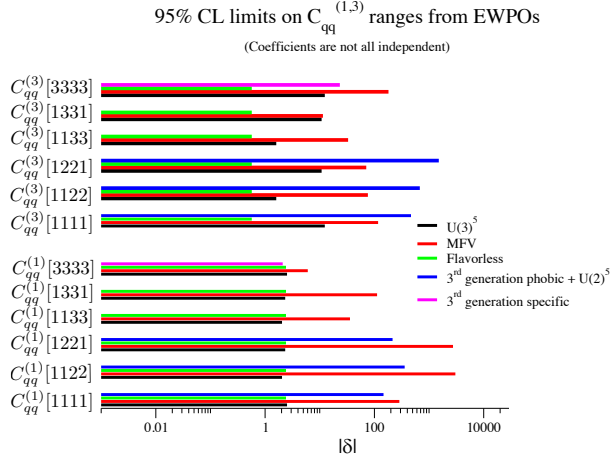


Figure 8. Limits on sample of coefficients of Class B 4-fermion operators in various flavor scenarios. δ is the range of the 95% confidence level limits. Only a single operator is taken to be non-zero and the flavor structures not shown are marginalized over. Exact numbers are given in Table V.

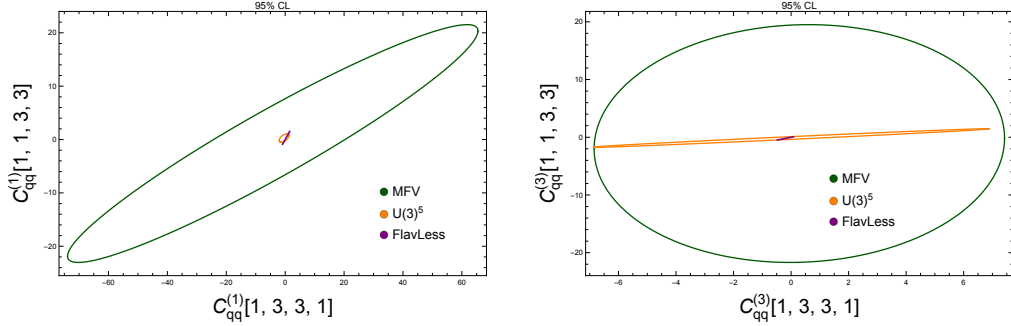


Figure 9. 95% CL limits on $C_{qq}^{(1)}$ (left) and $C_{qq}^{(3)}$ (right), in various flavor scenarios with all other coefficients taken to be 0. **On the left** we present $C_{qq}^{(1)}[1331]$ vs. $C_{qq}^{(1)}[1133]$ in the MFV (green), 3^{rd} generation centric (orange) and flavorless (violet) scenarios. **On the right** we present $C_{qq}^{(3)}[1331]$ vs. $C_{qq}^{(3)}[1133]$ in the MFV (green), 3^{rd} generation centric (orange) and flavorless (violet) scenarios. All the independent flavor structures not present in the plots are marginalized over.

level involve 2 fermions and the NLO corrections are typically quite small relative to the LO results. Comparing the NLO bounds on 2-fermion operators in different flavor scenarios results in factors of $\mathcal{O}(2)$.

However, the flavor structure has a dramatic effect on the bounds derived on the 4-fermion operators which first contribute to EWPOs at NLO. We present results for 4-fermion operators when the different flavor structures of an operator are marginalized over and observe large deviations in the fits for different flavor scenarios. These large effects result from the significant correlations between the different flavor structures. We have explicitly demonstrated that ignoring flavor typically leads to much tighter bounds on the SMEFT coefficients than in a general flavor scenario.

We also notice that the presence of a top quark in the internal propagators generally leads to stronger constraints. As we pointed out, the effects coming from the inclusion of NLO contributions are larger for operators where the top quark can contribute in the loop corrections. Furthermore, the limits that can be obtained on the 4-fermion operator coefficients in the $U(3)$ scenario are often orders of magnitude stronger than those obtained in the 3^{rd} generation phobic + $U(2)^5$ scenario. Since these scenarios have the same number of independent coefficients, the difference cannot be attributed to the marginalization procedure. Moreover, in the case of \mathcal{O}_{ll} , \mathcal{O}_{ee} and \mathcal{O}_{le} , where we do not expect an enhancement due to top loops, the two scenarios produce bounds with similar order of magnitudes.

At tree level, many of these 4-fermion operators contribute to the well measured Drell Yan process[71–73]. The NLO and EW corrections to Drell Yan production can potentially be combined with the EWPOs studied here to further improve the precision of the limits on the SMEFT coefficients[34, 74–77].

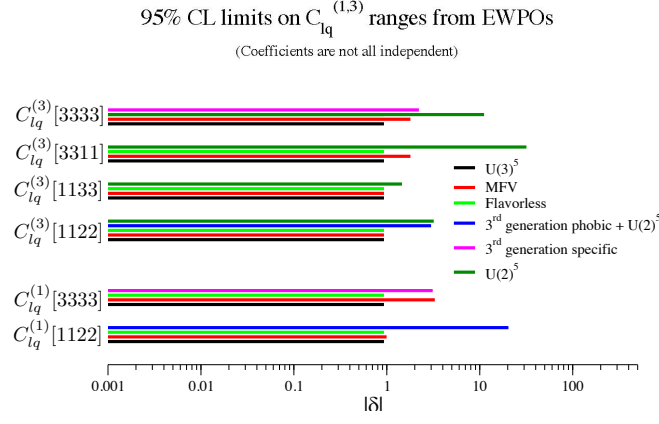


Figure 10. Limits on sample of coefficients of Class C 4-fermion operators in various flavor scenarios, with the independent flavor structures of each operator marginalized over. Exact numbers are given in VI.

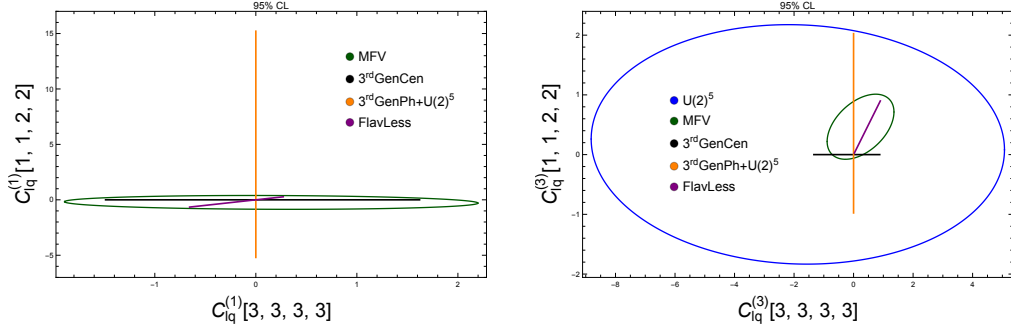


Figure 11. 95% CL limits on $C_{lq}^{(1)}$ (left) and $C_{lq}^{(3)}$ (right), in various flavor scenarios with all other coefficients taken to be 0. **On the left** we present $C_{lq}^{(1)}[3333]$ vs. $C_{lq}^{(1)}[1122]$ in the MFV (green), 3^{rd} generation centric (black), 3^{rd} generation phobic + $U(2)^5$ (orange) and flavorless (violet) scenarios. **On the right** we present $C_{lq}^{(3)}[3333]$ vs. $C_{lq}^{(3)}[1122]$ in the $U(2)^5$ (blue), MFV (green), 3^{rd} generation centric (black), 3^{rd} generation phobic + $U(2)^5$ (orange) and flavorless (violet) scenarios.. All the independent flavor structures not present in the plots are marginalized over.

Numerical results for the EWPOs to NLO in the QCD and EW interactions for a completely arbitrary flavor structure of the 2-fermion and 4-fermion operators are presented in the supplemental material. The supplemental material also contains numerical results for $H \rightarrow \gamma\gamma$ and $h \rightarrow Z\gamma$ to NLO in the QCD and EW interactions for a completely arbitrary flavor structure of the 2-fermion and 4-fermion operators, generalizing the results of [26, 27]. In the case of the Higgs decays, the effects of the flavor structure are small.

ACKNOWLEDGEMENTS

We thank A. Biekötter, B. Pecjak, D. Scott, and T. Smith for a detailed comparison of the NLO EW results for the EWPOs. L.B. would like to thank A. Brossa Gonzalo for helpful discussions. S.D. is supported by the U.S. Department of Energy under Grant Contract de-sc0012704. The work of L.B. and P.P.G. has received financial support from Xunta de Galicia (Centro singular de investigación de Galicia accreditation 2019-2022), by European Union ERDF, and by “María de Maeztu” Units of Excellence program MDM-2016-0692 and the Spanish Research

Operator	LO $U(3)^5$	NLO $U(3)^5$	LO MFV	NLO MFV	3 rd gen centric LO	3 rd gen centric NLO
$\mathcal{C}_{\phi q}^{(3)}$ [33]	[-0.0029,0.020]	[-0.0024,0.020]	[-0.019,0.042]	[-0.019,0.069]	[-0.011,0.045]	[-0.0062,0.069]
$\mathcal{C}_{\phi q}^{(3)}$ [11]	[-0.0029,0.020]*	[-0.0024,0.020]*	[-0.0093,0.024]	[-0.012,0.020]	0	0
$\mathcal{C}_{\phi q}^{(1)}$ [33]	[-0.0070,0.060]	[-0.011,0.053]	[-0.0067,0.060]	[-0.027,0.055]	[-0.011,0.045]	[-0.016,0.059]
$\mathcal{C}_{\phi q}^{(1)}$ [11]	[-0.0070,0.060]*	[-0.011,0.053]*	[-0.032,0.10]	[-0.071,0.18]	0	0
$\mathcal{C}_{\phi u}$ [33]	[-0.021,0.13]*	[-0.0037,0.11]	-	[-0.042,0.27]	-	[-0.020,0.29]
$\mathcal{C}_{\phi u}$ [11]	[-0.021,0.13]	[-0.0037,0.11]*	[-0.021,0.13]	[-0.031,0.10]	0	0
$\mathcal{C}_{\phi d}$ [33]	[-0.21,-0.0024]	[-0.18,0.0036]	[-0.21,-0.0024]	[-0.18,0.0036]	[-0.28,0.012]	[-0.37,0.00083]
$\mathcal{C}_{\phi e}$ [33]	[-0.0033,0.019]	[-0.0036,0.018]	[-0.0033,0.019]	[-0.0036,0.018]	[-0.040,0.028]	[-0.041,0.022]
$\mathcal{C}_{\phi l}^{(1)}$ [33]	[-0.011,0.0050]	[-0.012,0.0049]	[-0.011,0.0050]	[-0.012,0.0049]	[-0.026,0.033]	[-0.029,0.029]
$\mathcal{C}_{\phi l}^{(3)}$ [33]	[-0.015,-0.00041]	[-0.013,-0.00029]	[-0.015,-0.00041]	[-0.013,-0.00029]	[-0.020,0.033]	[-0.022,0.031]
\mathcal{C}_{uW} [33]	0	0	-	[-0.90,0.15]	-	[-0.90,0.15]
\mathcal{C}_{uB} [33]	0	0	-	[-0.61,0.061]	-	[-0.61,0.061]

Table IV. 95% CL allowed ranges on 2-fermion operators with varying flavor assumptions described in the text. Other flavor structure of a given operator are marginalized over, and different coefficients set to 0. The entries labelled with a "-" correspond to operators that do not contribute, while those labelled with a "*" are not independent. The flavor structures given not in the table can be always derived from those in the table using the relations detailed in the text.

State Agency.

-
- [1] I. Brivio and M. Trott, "The Standard Model as an Effective Field Theory," *Phys. Rept.* **793** (2019) 1–98, [arXiv:1706.08945 \[hep-ph\]](#).
- [2] A. Dedes, W. Materkowska, M. Paraskevas, J. Rosiek, and K. Suxho, "Feynman rules for the Standard Model Effective Field Theory in R_ξ -gauges," *JHEP* **06** (2017) 143, [arXiv:1704.03888 \[hep-ph\]](#).
- [3] J. de Blas, J. C. Criado, M. Perez-Victoria, and J. Santiago, "Effective description of general extensions of the Standard Model: the complete tree-level dictionary," *JHEP* **03** (2018) 109, [arXiv:1711.10391 \[hep-ph\]](#).
- [4] J. Brehmer, A. Freitas, D. Lopez-Val, and T. Plehn, "Pushing Higgs Effective Theory to its Limits," *Phys. Rev. D* **93** no. 7, (2016) 075014, [arXiv:1510.03443 \[hep-ph\]](#).
- [5] S. Dawson, S. Homiller, and S. D. Lane, "Putting standard model EFT fits to work," *Phys. Rev. D* **102** no. 5, (2020) 055012, [arXiv:2007.01296 \[hep-ph\]](#).
- [6] T. Corbett, A. Helset, A. Martin, and M. Trott, "EWPD in the SMEFT to dimension eight," *JHEP* **06** (2021) 076, [arXiv:2102.02819 \[hep-ph\]](#).
- [7] I. Brivio, "SMEFTsim 3.0 — a practical guide," *JHEP* **04** (2021) 073, [arXiv:2012.11343 \[hep-ph\]](#).
- [8] I. Brivio, Y. Jiang, and M. Trott, "The SMEFTsim package, theory and tools," *JHEP* **12** (2017) 070, [arXiv:1709.06492 \[hep-ph\]](#).
- [9] C. Degrande, G. Durieux, F. Maltoni, K. Mimasu, E. Vryonidou, and C. Zhang, "Automated one-loop computations in the standard model effective field theory," *Phys. Rev. D* **103** no. 9, (2021) 096024, [arXiv:2008.11743 \[hep-ph\]](#).
- [10] **SMEFT** Collaboration, J. J. Ethier, G. Magni, F. Maltoni, L. Mantani, E. R. Nocera, J. Rojo, E. Slade, E. Vryonidou, and C. Zhang, "Combined SMEFT interpretation of Higgs, diboson, and top quark data from the LHC," *JHEP* **11** (2021) 089, [arXiv:2105.00006 \[hep-ph\]](#).
- [11] J. Ellis, M. Madigan, K. Mimasu, V. Sanz, and T. You, "Top, Higgs, Diboson and Electroweak Fit to the Standard Model Effective Field Theory," *JHEP* **04** (2021) 279, [arXiv:2012.02779 \[hep-ph\]](#).
- [12] A. Biekötter, T. Corbett, and T. Plehn, "The Gauge-Higgs Legacy of the LHC Run II," *SciPost Phys.* **6** no. 6, (2019) 064, [arXiv:1812.07587 \[hep-ph\]](#).
- [13] E. Bagnaschi, J. Ellis, M. Madigan, K. Mimasu, V. Sanz, and T. You, "SMEFT analysis of m_W ," *JHEP* **08** (2022) 308, [arXiv:2204.05260 \[hep-ph\]](#).
- [14] J. Ellis, C. W. Murphy, V. Sanz, and T. You, "Updated Global SMEFT Fit to Higgs, Diboson and Electroweak Data," *JHEP* **06** (2018) 146, [arXiv:1803.03252 \[hep-ph\]](#).
- [15] I. Brivio *et al.*, "Truncation, validity, uncertainties," [arXiv:2201.04974 \[hep-ph\]](#).

Operator	$U(3)^5$	MFV	$U(2)^5$	3^{rd} gen specific	3^{rd} gen phobic	3^{rd} gen phobic+ $U(2)^5$	Flavorless
$\mathcal{C}_{qq}^{(3)}[1133]$	[-0.80,0.81]	[-17.6,15.4]	x	0	0	0	[-0.48,0.09]
$\mathcal{C}_{qq}^{(3)}[1331]$	[-4.38,6.42]	[-5.43,6.00]	x	0	0	0	[-0.48,0.09]*
$\mathcal{C}_{qq}^{(3)}[1122]$	[-0.80,0.81]*	[-31.2,45.4]	x	0	x	[-303,375]	[-0.48,0.09]*
$\mathcal{C}_{qq}^{(3)}[1221]$	[-4.38,6.42]*	[-44.8,26.3]	x	0	x	[-836,672]	[-0.48,0.09]*
$\mathcal{C}_{qq}^{(3)}[3333]$	[-5.15,7.21]*	[-89.4,90.5]*	x	[-2.94,20.4]	0	0	[-0.48,0.09]*
$\mathcal{C}_{qq}^{(3)}[1111]$	[-5.15,7.21]*	[-60.9,56.6]*	x	0	x	[-460,369]*	[-0.48,0.09]*
$\mathcal{C}_{qq}^{(1)}[1133]$	[-0.20,1.84]	[-18.6,17.1]	x	0	0	0	[-0.89,1.52]
$\mathcal{C}_{qq}^{(1)}[1331]$	[-1.39,0.94]	[-60.0,51.6]	x	0	0	0	[-0.89,1.52]*
$\mathcal{C}_{qq}^{(1)}[1122]$	[-0.20,1.84]*	[-1623,1408]	x	0	x	[-189,169]	[-0.89,1.52]*
$\mathcal{C}_{qq}^{(1)}[1221]$	[-1.39,0.94]*	[-1276,1470]	x	0	x	[-109,106]	[-0.89,1.52]*
$\mathcal{C}_{qq}^{(1)}[3333]$	[-0.66,1.86]*	[-2.62,3.42]*	x	[-0.26,1.84]	0	0	[-0.89,1.52]*
$\mathcal{C}_{qq}^{(1)}[1111]$	[-0.66,1.86]*	[-153,133]*	x	0	x	[-85.0,62.3]*	[-0.89,1.52]*
$\mathcal{C}_u[1133]$	[-5.65,2.52]	[-5.65,2.52]	[-46.1,22.2]	0	0	0	[-.0029,.021]
$\mathcal{C}_u[1331]$	[-0.076,0.047]	[-0.076,0.047]	[-38.2,65.4]	0	0	0	[-.0029,.021]*
$\mathcal{C}_u[1122]$	[-5.65,2.52]*	[-5.65,2.52]*	[-18.4,14.2]	0	[-11.4,17.4]	[-9.3,5.3]	[-.0029,.021]*
$\mathcal{C}_u[1221]$	[-0.076,0.047]*	[-0.076,0.047]*	[-0.25,0.22]	0	[-0.16,0.27]	[-0.13,0.088]	[-.0029,.021]*
$\mathcal{C}_u[3333]$	[-5.72,2.56]*	[-5.72,2.56]*	[-44.0,191]	[-55.2,41.6]	0	0	[-.0029,.021]*
$\mathcal{C}_u[2222]$	[-5.72,2.56]*	[-5.72,2.56]*	[-18.6,14.4]*	0	[-90.2,27.0]	[-9.4,5.4]*	[-.0029,.021]*
$\mathcal{C}_u[1111]$	[-5.72,2.56]*	[-5.72,2.56]*	[-18.6,14.4]*	0	[-26.7,26.3]	[-9.4,5.4]*	[-.0029,.021]*
$\mathcal{C}_{ee}[1133]$	[-0.80,4.07]	[-0.80,4.07]	x	0	0	0	[-1.07,5.4]
$\mathcal{C}_{ee}[1122]$	[-0.80,4.07]*	[-0.80,4.07]*	x	0	x	[-0.67,6.02]	[-1.07,5.4]*
$\mathcal{C}_{ee}[3333]$	[-1.60,8.13]*	[-1.60,8.13]*	x	[-36.7,19.7]	0	0	[-1.07,5.4]*
$\mathcal{C}_{ee}[1111]$	[-0.80,4.07]*	[-0.80,4.07]*	x	0	x	[-1.34,12.0]	[-1.07,5.4]*
$\mathcal{C}_{uu}[1133]$	x	x	x	x	x	x	[-1.67,0.30]
$\mathcal{C}_{dd}[3333]$	x	x	x	[-428,5.54]	x	x	[-68.4,2.38]

Table V. NLO results for 95% CL limits on Class B operators when the coefficients of all other operators are set to 0 and the different flavor structures of a given operator are marginalized over. The limits marked with a "*" are obtained using the relations given in the text and do not represent independent coefficients. We label with an "x" the cases where no limit can be derived.

- [16] A. Efrati, A. Falkowski, and Y. Soreq, "Electroweak constraints on flavorful effective theories," *JHEP* **07** (2015) 018, [arXiv:1503.07872 \[hep-ph\]](#).
- [17] A. Falkowski and D. Straub, "Flavourful SMEFT likelihood for Higgs and electroweak data," *JHEP* **04** (2020) 066, [arXiv:1911.07866 \[hep-ph\]](#).
- [18] A. Greljo, A. Palavrić, and A. E. Thomsen, "Adding Flavor to the SMEFT," *JHEP* **10** (2022) 010, [arXiv:2203.09561 \[hep-ph\]](#).
- [19] D. A. Faroughy, G. Isidori, F. Wilsch, and K. Yamamoto, "Flavour symmetries in the SMEFT," *JHEP* **08** (2020) 166, [arXiv:2005.05366 \[hep-ph\]](#).

Operator	$U(3)^5$	MFV	$U(2)^5$	3^{rd} gen specific	3^{rd} gen phobic + $U(2)^5$	Flavorless
$\mathcal{C}_{lq}^{(3)}[1133]$	[0.026,0.90]	[0.03,0.90]	[-0.0078,1.45]	0	0	[0.026,0.90]
$\mathcal{C}_{lq}^{(3)}[3311]$	[0.026,0.90]*	[-0.66,1.13]	[-9.62,22.2]	0	0	[0.026,0.90]*
$\mathcal{C}_{lq}^{(3)}[1122]$	[0.026,0.90]*	[0.03,0.90]*	[-1.43,1.78]	0	[-0.98,2.02]	[0.026,0.90]*
$\mathcal{C}_{lq}^{(3)}[3333]$	[0.026,0.90]*	[-0.66,1.13]*	[-7.43,3.69]	[-1.33,0.88]	0	[0.026,0.90]*
$\mathcal{C}_{lq}^{(1)}[1122]$	[-0.66,0.27]	[-0.73,0.27]	x	0	[-5.20,15.2]	[-0.66,0.27]
$\mathcal{C}_{lq}^{(1)}[3333]$	[-0.66,0.27]*	[-1.50,1.79]	x	[-1.50,1.62]	0	[-0.66,0.27]*
$\mathcal{C}_{lu}[1122]$	[-0.20,0.49]	[-0.20,0.55]	x	0	[-2.6,7.6]	[-0.20,0.49]
$\mathcal{C}_{lu}[3333]$	[-0.20,0.49]*	[-1.33,1.13]	x	[-1.35,1.27]	0	[-0.20,0.49]*
$\mathcal{C}_{qe}[1122]$	[-0.20,1.06]	[-66.2,142]	x	0	[-25.7,3.34]	[-0.20,1.06]
$\mathcal{C}_{qe}[3333]$	[-0.20,1.06]*	[-2.38,6.35]	x	[-2.26,1.25]	0	[-0.20,1.06]*
$\mathcal{C}_{ed}[1122]$	[-3.86,15.3]	[-3.86,15.3]	x	0	[-3.29,25.8]	[-3.86,15.3]
$\mathcal{C}_{ed}[3333]$	[-3.86,15.3]*	[-3.86,15.3]*	x	[-117,42.8]	0	[-3.86,15.3]*
$\mathcal{C}_{ld}[1122]$	[-9.11,3.26]	[-9.11,3.26]	x	0	[-15.2,5.21]	[-9.11,3.26]
$\mathcal{C}_{ld}[3333]$	[-9.11,3.26]*	[-9.11,3.26]*	x	[-72.9,59.3]	0	[-9.11,3.26]*
$\mathcal{C}_{le}[1122]$	[-7.09,8.13]	[-7.09,8.13]	x	0	[-10.5,14.5]	[-7.09,8.13]
$\mathcal{C}_{le}[3333]$	[-7.09,8.13]*	[-7.09,8.13]*	x	[-92.8,55.5]	0	[-7.09,8.13]*
$\mathcal{C}_{eu}[1122]$	[-0.81,0.16]	[-0.88,0.11]	x	0	[-12.9,1.66]	[-0.81,0.16]
$\mathcal{C}_{eu}[3333]$	[-0.81,0.16]*	[-1.07,1.73]	x	[-1.05,1.95]	0	[-0.81,0.16]*
$\mathcal{C}_{ud}^{(1)}[1122]$	[-0.30,7.68]	[-154,90.2]	x	0	[-13.9,75.7]	[-0.30,7.68]
$\mathcal{C}_{ud}^{(1)}[3333]$	[-0.30,7.68]*	[-9.3,27.0]	x	[-0.24,18.4]	0	[-0.30,7.68]*
$\mathcal{C}_{qd}^{(1)}[1122]$	[-13.3,0.47]	[-202,128]	x	0	[-29.4,139]	[-13.3,0.47]
$\mathcal{C}_{qd}^{(1)}[3333]$	[-13.3,0.47]*	[-27.2,8.27]	x	[-24.4,0.11]	0	[-13.3,0.47]*
$\mathcal{C}_{qu}^{(1)}[1122]$	[-2.82,0.54]	x	x	0	[-71.0,14.1]	[-2.82,0.54]
$\mathcal{C}_{qu}^{(1)}[3333]$	[-2.82,0.54]*	x	x	[-3.07,0.44]	0	[-2.82,0.54]*

Table VI. NLO results for 95% CL limits on Class C operators when the coefficients of all other operators are set to 0 and the different flavor structures of a given operator are marginalized over. The limits marked with a "*" are obtained using the relations given in the text and do not represent independent coefficients. We label with an "x" the cases where no limit can be derived.

- [20] S. Bruggisser, R. Schäfer, D. van Dyk, and S. Westhoff, "The Flavor of UV Physics," *JHEP* **05** (2021) 257, [arXiv:2101.07273 \[hep-ph\]](#).
- [21] A. Crivellin, F. Kirk, C. A. Manzari, and M. Montull, "Global Electroweak Fit and Vector-Like Leptons in Light of the Cabibbo Angle Anomaly," *JHEP* **12** (2020) 166, [arXiv:2008.01113 \[hep-ph\]](#).
- [22] A. Crivellin, M. Kirk, T. Kitahara, and F. Mescia, "Global fit of modified quark couplings to EW gauge bosons and vector-like quarks in light of the Cabibbo angle anomaly," *JHEP* **03** (2023) 234, [arXiv:2212.06862 \[hep-ph\]](#).
- [23] E. E. Jenkins, A. V. Manohar, and M. Trott, "Renormalization Group Evolution of the Standard Model Dimension Six Operators I: Formalism and lambda Dependence," *JHEP* **10** (2013) 087, [arXiv:1308.2627 \[hep-ph\]](#).
- [24] E. E. Jenkins, A. V. Manohar, and M. Trott, "Renormalization Group Evolution of the Standard Model Dimension Six Operators II: Yukawa Dependence," *JHEP* **01** (2014) 035, [arXiv:1310.4838 \[hep-ph\]](#).

- [25] R. Alonso, E. E. Jenkins, A. V. Manohar, and M. Trott, “Renormalization Group Evolution of the Standard Model Dimension Six Operators III: Gauge Coupling Dependence and Phenomenology,” *JHEP* **04** (2014) 159, [arXiv:1312.2014 \[hep-ph\]](#).
- [26] S. Dawson and P. P. Giardino, “Higgs decays to ZZ and $Z\gamma$ in the standard model effective field theory: An NLO analysis,” *Phys. Rev.* **D97** no. 9, (2018) 093003, [arXiv:1801.01136 \[hep-ph\]](#).
- [27] S. Dawson and P. P. Giardino, “Electroweak corrections to Higgs boson decays to $\gamma\gamma$ and W^+W^- in standard model EFT,” *Phys. Rev.* **D98** no. 9, (2018) 095005, [arXiv:1807.11504 \[hep-ph\]](#).
- [28] J. M. Cullen and B. D. Pecjak, “Higgs decay to fermion pairs at NLO in SMEFT,” *JHEP* **11** (2020) 079, [arXiv:2007.15238 \[hep-ph\]](#).
- [29] A. Dedes, K. Suxho, and L. Trifyllis, “The decay $h \rightarrow Z\gamma$ in the Standard-Model Effective Field Theory,” *JHEP* **06** (2019) 115, [arXiv:1903.12046 \[hep-ph\]](#).
- [30] A. Dedes, M. Paraskevas, J. Rosiek, K. Suxho, and L. Trifyllis, “The decay $h \rightarrow \gamma\gamma$ in the Standard-Model Effective Field Theory,” *JHEP* **08** (2018) 103, [arXiv:1805.00302 \[hep-ph\]](#).
- [31] C. Hartmann, W. Shepherd, and M. Trott, “The Z decay width in the SMEFT: y_t and λ corrections at one loop,” *JHEP* **03** (2017) 060, [arXiv:1611.09879 \[hep-ph\]](#).
- [32] C. Hartmann and M. Trott, “Higgs Decay to Two Photons at One Loop in the Standard Model Effective Field Theory,” *Phys. Rev. Lett.* **115** no. 19, (2015) 191801, [arXiv:1507.03568 \[hep-ph\]](#).
- [33] S. Dawson and P. P. Giardino, “Electroweak and QCD corrections to Z and W pole observables in the standard model EFT,” *Phys. Rev. D* **101** no. 1, (2020) 013001, [arXiv:1909.02000 \[hep-ph\]](#).
- [34] S. Dawson and A. Ismail, “Standard model EFT corrections to Z boson decays,” *Phys. Rev.* **D98** no. 9, (2018) 093003, [arXiv:1808.05948 \[hep-ph\]](#).
- [35] S. Dawson and P. P. Giardino, “Flavorful electroweak precision observables in the Standard Model effective field theory,” *Phys. Rev. D* **105** no. 7, (2022) 073006, [arXiv:2201.09887 \[hep-ph\]](#).
- [36] I. Brivio, S. Bruggisser, F. Maltoni, R. Moutafis, T. Plehn, E. Vryonidou, S. Westhoff, and C. Zhang, “O new physics, where art thou? A global search in the top sector,” *JHEP* **02** (2020) 131, [arXiv:1910.03606 \[hep-ph\]](#).
- [37] L. Alasfar, A. Azatov, J. de Blas, A. Paul, and M. Valli, “ B anomalies under the lens of electroweak precision,” *JHEP* **12** (2020) 016, [arXiv:2007.04400 \[hep-ph\]](#).
- [38] R. Boughezal, C.-Y. Chen, F. Petriello, and D. Wiegand, “Top quark decay at next-to-leading order in the Standard Model Effective Field Theory,” [arXiv:1907.00997 \[hep-ph\]](#).
- [39] S. Bruggisser, D. van Dyk, and S. Westhoff, “Resolving the flavor structure in the MFV-SMEFT,” *JHEP* **02** (2023) 225, [arXiv:2212.02532 \[hep-ph\]](#).
- [40] B. Grzadkowski, M. Iskrzynski, M. Misiak, and J. Rosiek, “Dimension-Six Terms in the Standard Model Lagrangian,” *JHEP* **10** (2010) 085, [arXiv:1008.4884 \[hep-ph\]](#).
- [41] G. D’Ambrosio, G. F. Giudice, G. Isidori, and A. Strumia, “Minimal flavor violation: An Effective field theory approach,” *Nucl. Phys. B* **645** (2002) 155–187, [arXiv:hep-ph/0207036](#).
- [42] A. Crivellin, M. Hoferichter, M. Kirk, C. A. Manzari, and L. Schnell, “First-generation new physics in simplified models: from low-energy parity violation to the LHC,” *JHEP* **10** (2021) 221, [arXiv:2107.13569 \[hep-ph\]](#).
- [43] J. Baglio, S. Dawson, and I. M. Lewis, “An NLO QCD effective field theory analysis of W^+W^- production at the LHC including fermionic operators,” *Phys. Rev. D* **96** no. 7, (2017) 073003, [arXiv:1708.03332 \[hep-ph\]](#).
- [44] I. Brivio and M. Trott, “Scheming in the SMEFT... and a reparameterization invariance!,” *JHEP* **07** (2017) 148, [arXiv:1701.06424 \[hep-ph\]](#). [Addendum: *JHEP* 05, 136 (2018)].
- [45] A. Alloul, N. D. Christensen, C. Degrande, C. Duhr, and B. Fuks, “FeynRules 2.0 - A complete toolbox for tree-level phenomenology,” *Comput. Phys. Commun.* **185** (2014) 2250–2300, [arXiv:1310.1921 \[hep-ph\]](#).
- [46] T. Hahn, “Generating Feynman diagrams and amplitudes with FeynArts 3,” *Comput. Phys. Commun.* **140** (2001) 418–431, [arXiv:hep-ph/0012260 \[hep-ph\]](#).
- [47] R. Mertig, M. Bohm, and A. Denner, “FEYN CALC: Computer algebraic calculation of Feynman amplitudes,” *Comput. Phys. Commun.* **64** (1991) 345–359.
- [48] V. Shtabovenko, R. Mertig, and F. Orellana, “New Developments in FeynCalc 9.0,” *Comput. Phys. Commun.* **207** (2016) 432–444, [arXiv:1601.01167 \[hep-ph\]](#).
- [49] G. Passarino and M. J. G. Veltman, “One Loop Corrections for e^+e^- Annihilation Into $\mu^+\mu^-$ in the Weinberg Model,” *Nucl. Phys. B* **160** (1979) 151–207.
- [50] C. Anastasiou and K. Melnikov, “Higgs boson production at hadron colliders in NNLO QCD,” *Nucl. Phys.* **B646** (2002) 220–256, [arXiv:hep-ph/0207004 \[hep-ph\]](#).
- [51] O. V. Tarasov, “Generalized recurrence relations for two loop propagator integrals with arbitrary masses,” *Nucl. Phys.* **B502** (1997) 455–482, [arXiv:hep-ph/9703319 \[hep-ph\]](#).
- [52] S. P. Martin, “Evaluation of two loop selfenergy basis integrals using differential equations,” *Phys. Rev.* **D68** (2003) 075002, [arXiv:hep-ph/0307101 \[hep-ph\]](#).

- [53] A. V. Smirnov, “FIRE5: a C++ implementation of Feynman Integral REduction,” *Comput. Phys. Commun.* **189** (2015) 182–191, [arXiv:1408.2372 \[hep-ph\]](#).
- [54] W. F. L. Hollik, “Radiative Corrections in the Standard Model and their Role for Precision Tests of the Electroweak Theory,” *Fortsch. Phys.* **38** (1990) 165–260.
- [55] G. Degrandi, P. Gambino, and P. P. Giardino, “The $m_W - m_Z$ interdependence in the Standard Model: a new scrutiny,” *JHEP* **05** (2015) 154, [arXiv:1411.7040 \[hep-ph\]](#).
- [56] I. Brivio, S. Dawson, J. de Blas, G. Durieux, P. Savard, A. Denner, A. Freitas, C. Hays, B. Pecjak, and A. Vicini, “Electroweak input parameters,” [arXiv:2111.12515 \[hep-ph\]](#).
- [57] C.-Y. Chen, S. Dawson, and C. Zhang, “Electroweak Effective Operators and Higgs Physics,” *Phys. Rev.* **D89** no. 1, (2014) 015016, [arXiv:1311.3107 \[hep-ph\]](#).
- [58] M. Ghezzi, R. Gomez-Ambrosio, G. Passarino, and S. Uccirati, “NLO Higgs effective field theory and κ -framework,” *JHEP* **07** (2015) 175, [arXiv:1505.03706 \[hep-ph\]](#).
- [59] **Particle Data Group** Collaboration, “Review of particle physics,” *Phys. Rev. D* **98** (Aug, 2018) 030001. <https://link.aps.org/doi/10.1103/PhysRevD.98.030001>.
- [60] J. R. Espinosa, M. Muhlleitner, C. Grojean, and M. Trott, “Probing for Invisible Higgs Decays with Global Fits,” *JHEP* **09** (2012) 126, [arXiv:1205.6790 \[hep-ph\]](#).
- [61] L. Berthier and M. Trott, “Consistent constraints on the Standard Model Effective Field Theory,” *JHEP* **02** (2016) 069, [arXiv:1508.05060 \[hep-ph\]](#).
- [62] A. Freitas, “Higher-order electroweak corrections to the partial widths and branching ratios of the Z boson,” *JHEP* **04** (2014) 070, [arXiv:1401.2447 \[hep-ph\]](#).
- [63] I. Dubovyk, A. Freitas, J. Gluza, T. Riemann, and J. Usovitsch, “Complete electroweak two-loop corrections to Z boson production and decay,” *Phys. Lett.* **B783** (2018) 86–94, [arXiv:1804.10236 \[hep-ph\]](#).
- [64] I. Dubovyk, A. Freitas, J. Gluza, T. Riemann, and J. Usovitsch, “Electroweak pseudo-observables and Z-boson form factors at two-loop accuracy,” [arXiv:1906.08815 \[hep-ph\]](#).
- [65] M. Awramik, M. Czakon, and A. Freitas, “Electroweak two-loop corrections to the effective weak mixing angle,” *JHEP* **11** (2006) 048, [arXiv:hep-ph/0608099 \[hep-ph\]](#).
- [66] M. Awramik, M. Czakon, A. Freitas, and B. A. Kniehl, “Two-loop electroweak fermionic corrections to $\sin^2 \theta_{\text{eff}}^{\text{anti-b}}$,” *Nucl. Phys.* **B813** (2009) 174–187, [arXiv:0811.1364 \[hep-ph\]](#).
- [67] M. Awramik, M. Czakon, A. Freitas, and G. Weiglein, “Precise prediction for the W boson mass in the standard model,” *Phys. Rev.* **D69** (2004) 053006, [arXiv:hep-ph/0311148 \[hep-ph\]](#).
- [68] J. Erler and M. Schott, “Electroweak Precision Tests of the Standard Model after the Discovery of the Higgs Boson,” *Prog. Part. Nucl. Phys.* **106** (2019) 68–119, [arXiv:1902.05142 \[hep-ph\]](#).
- [69] G.-C. Cho, K. Hagiwara, Y. Matsumoto, and D. Nomura, “The MSSM confronts the precision electroweak data and the muon $g-2$,” *JHEP* **11** (2011) 068, [arXiv:1104.1769 \[hep-ph\]](#).
- [70] Y. Liu, Y. Wang, C. Zhang, L. Zhang, and J. Gu, “Probing top-quark operators with precision electroweak measurements*,” *Chin. Phys. C* **46** no. 11, (2022) 113105, [arXiv:2205.05655 \[hep-ph\]](#).
- [71] J. de Blas, M. Chala, and J. Santiago, “Global Constraints on Lepton-Quark Contact Interactions,” *Phys. Rev. D* **88** (2013) 095011, [arXiv:1307.5068 \[hep-ph\]](#).
- [72] G. Panico, L. Ricci, and A. Wulzer, “High-energy EFT probes with fully differential Drell-Yan measurements,” [arXiv:2103.10532 \[hep-ph\]](#).
- [73] V. Cirigliano, M. Gonzalez-Alonso, and M. L. Graesser, “Non-standard Charged Current Interactions: beta decays versus the LHC,” *JHEP* **02** (2013) 046, [arXiv:1210.4553 \[hep-ph\]](#).
- [74] S. Dawson and P. P. Giardino, “New physics through Drell-Yan standard model EFT measurements at NLO,” *Phys. Rev. D* **104** no. 7, (2021) 073004, [arXiv:2105.05852 \[hep-ph\]](#).
- [75] R. Boughezal, Y. Huang, and F. Petriello, “Impact of high invariant-mass Drell-Yan forward-backward asymmetry measurements on SMEFT fits,” [arXiv:2303.08257 \[hep-ph\]](#).
- [76] R. Boughezal, Y. Huang, and F. Petriello, “Exploring the SMEFT at dimension eight with Drell-Yan transverse momentum measurements,” *Phys. Rev. D* **106** no. 3, (2022) 036020, [arXiv:2207.01703 \[hep-ph\]](#).
- [77] V. Bresó-Pla, A. Falkowski, and M. González-Alonso, “ A_{FB} in the SMEFT: precision Z physics at the LHC,” [arXiv:2103.12074 \[hep-ph\]](#).

Appendix A: Other plots for 2-fermion operators

In this appendix, we show a collection of plots involving the 2-fermion operators, as described in the text.

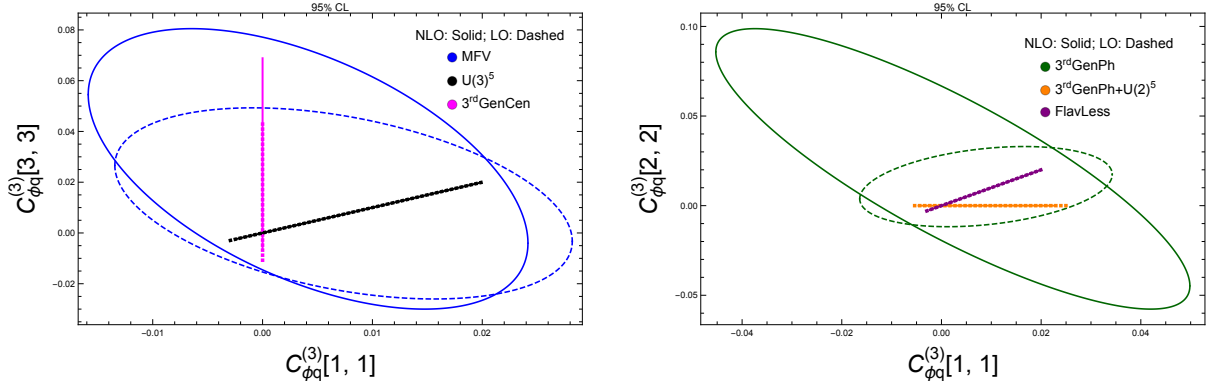


Figure 12. 95% CL limits on $C_{\phi q}^{(3)}[ij]$ under flavor assumptions described in the text. Results at LO are drawn with dashed lines, results at NLO are drawn with solid lines. **On the left** we present $C_{\phi q}^{(3)}[11]$ vs. $C_{\phi q}^{(3)}[33]$ in the $U(3)^5$ (black), MFV (blue) and 3^{rd} generation centric (magenta) scenarios. In these scenarios $C_{\phi q}^{(3)}[22] = C_{\phi q}^{(3)}[11]$. **On the right** we present $C_{\phi q}^{(3)}[11]$ vs. $C_{\phi q}^{(3)}[22]$ in the 3^{rd} generation phobic (green), 3^{rd} generation phobic + $U(2)^5$ (orange) and flavorless (violet) scenarios. In the first two scenarios $C_{\phi q}^{(3)}[33] = 0$, while in the flavorless scenario $C_{\phi q}^{(3)}[33] = C_{\phi q}^{(3)}[22] = C_{\phi q}^{(3)}[11]$. All other coefficients are set to 0.

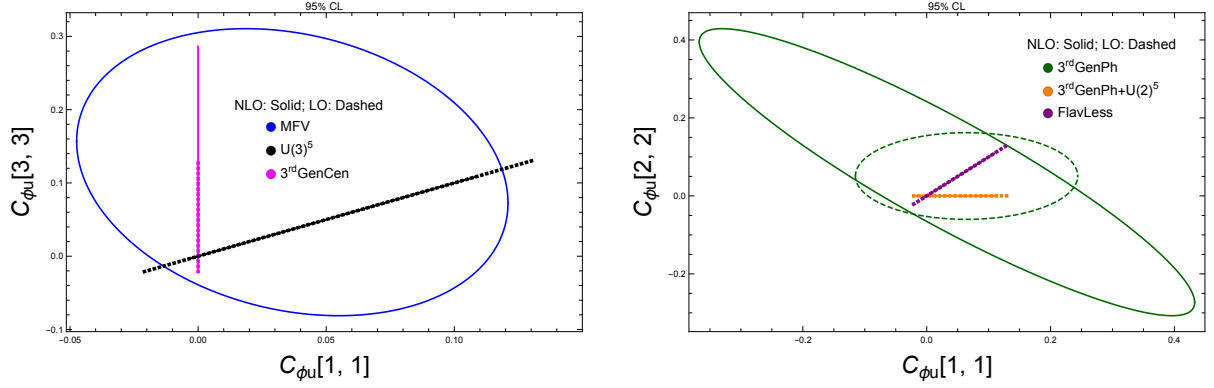


Figure 13. 95% CL limits on $C_{\phi u}[ij]$ under flavor assumptions described in the text. Results at LO are drawn with dashed lines, results at NLO are drawn with solid lines. **On the left** we present $C_{\phi u}[11]$ vs. $C_{\phi u}[33]$ in the $U(3)^5$ (black), MFV (blue) and 3^{rd} generation centric (magenta) scenarios. In these scenarios $C_{\phi u}[22] = C_{\phi u}[11]$, also notice that for the MFV scenario only the NLO results can be obtained. **On the right** we present $C_{\phi u}[11]$ vs. $C_{\phi u}[22]$ in the 3^{rd} generation phobic (green), 3^{rd} generation phobic + $U(2)^5$ (orange) and flavorless (violet) scenarios. In the first two scenarios $C_{\phi u}[33] = 0$, while in the flavorless scenario $C_{\phi u}[33] = C_{\phi u}[22] = C_{\phi u}[11]$. All other coefficients are set to 0.

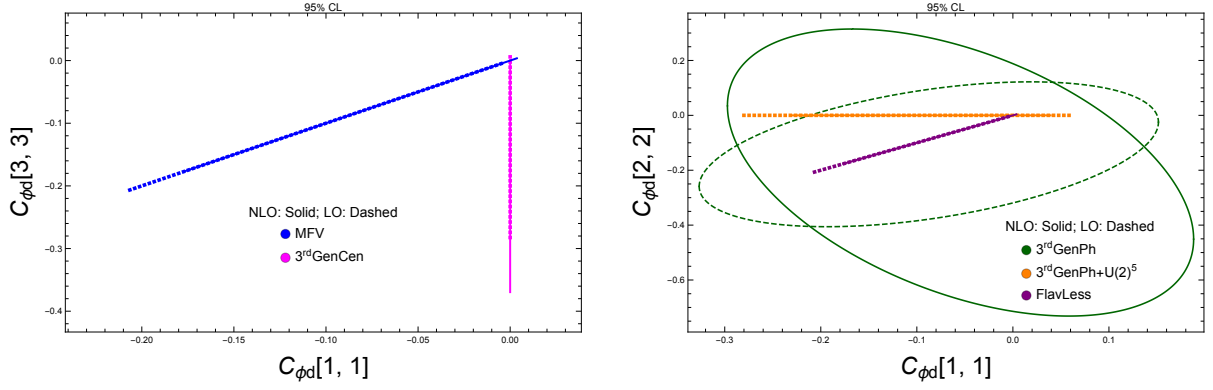


Figure 14. 95% CL limits on $C_{\phi d}[ij]$ under flavor assumptions described in the text. Results at LO are drawn with dashed lines, results at NLO are drawn with solid lines. **On the left** we present $C_{\phi d}[11]$ vs. $C_{\phi d}[33]$ in the MFV (blue) and 3^{rd} generation centric (magenta) scenarios. In these scenarios $C_{\phi d}[22] = C_{\phi d}[11]$. **On the right** we present $C_{\phi d}[11]$ vs. $C_{\phi d}[22]$ in the 3^{rd} generation phobic (green), 3^{rd} generation phobic + $U(2)^5$ (orange) and flavorless (violet) scenarios. In the first two scenarios $C_{\phi d}[33] = 0$, while in the flavorless scenario $C_{\phi d}[33] = C_{\phi d}[22] = C_{\phi d}[11]$. All other coefficients are set to 0.

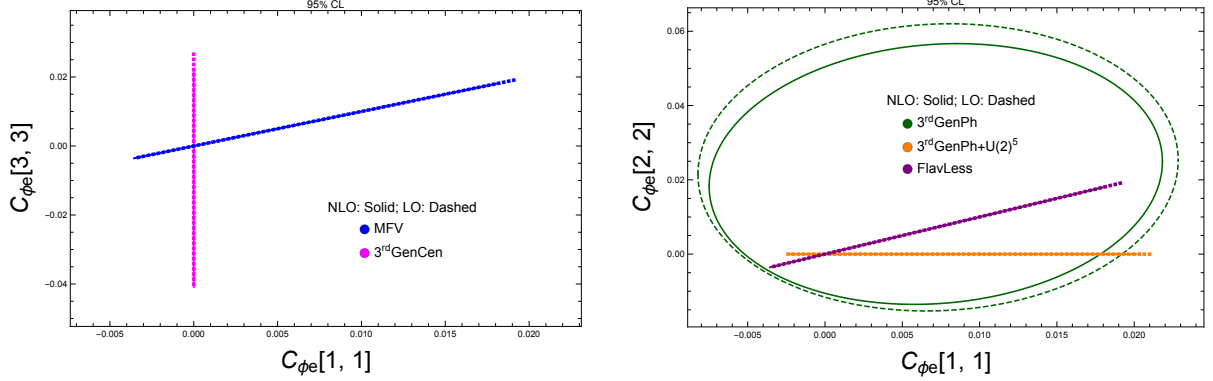


Figure 15. 95% CL limits on $C_{\phi e}[ij]$ under flavor assumptions described in the text. Results at LO are drawn with dashed lines, results at NLO are drawn with solid lines. **On the left** we present $C_{\phi e}[11]$ vs. $C_{\phi e}[33]$ in the MFV (blue) and 3^{rd} generation centric (magenta) scenarios. In these scenarios $C_{\phi e}[22] = C_{\phi e}[11]$. **On the right** we present $C_{\phi e}[11]$ vs. $C_{\phi e}[22]$ in the 3^{rd} generation phobic (green), 3^{rd} generation phobic + $U(2)^5$ (orange) and flavorless (violet) scenarios. In the first two scenarios $C_{\phi e}[33] = 0$, while in the flavorless scenario $C_{\phi e}[33] = C_{\phi e}[22] = C_{\phi e}[11]$. All other coefficients are set to 0.

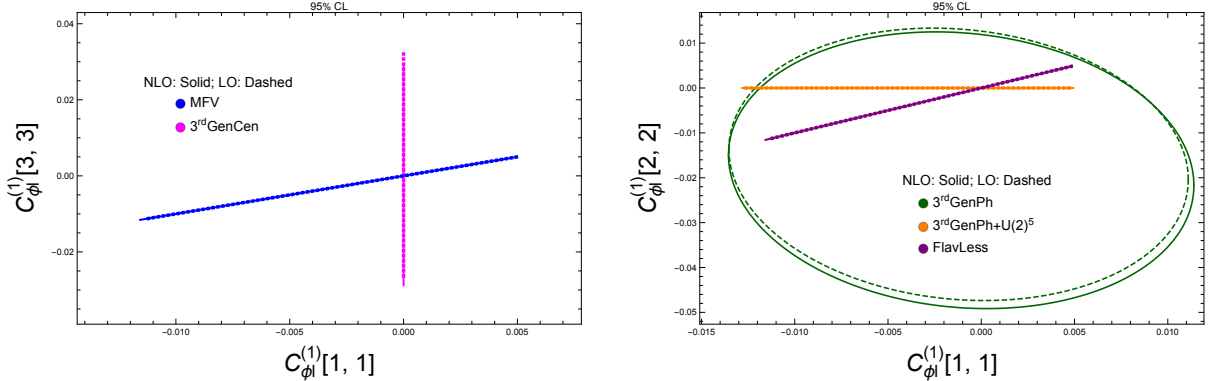


Figure 16. 95% CL limits on $C_{\phi l}^{(1)}[ij]$ under flavor assumptions described in the text. Results at LO are drawn with dashed lines, results at NLO are drawn with solid lines. **On the left** we present $C_{\phi l}^{(1)}[11]$ vs. $C_{\phi l}^{(1)}[33]$ in the MFV (blue) and 3^{rd} generation centric (magenta) scenarios. In these scenarios $C_{\phi l}^{(1)}[22] = C_{\phi l}^{(1)}[11]$. **On the right** we present $C_{\phi l}^{(1)}[11]$ vs. $C_{\phi l}^{(1)}[22]$ in the 3^{rd} generation phobic (green), 3^{rd} generation phobic + $U(2)^5$ (orange) and flavorless (violet) scenarios. In the first two scenarios $C_{\phi l}^{(1)}[33] = 0$, while in the flavorless scenario $C_{\phi l}^{(1)}[33] = C_{\phi l}^{(1)}[22] = C_{\phi l}^{(1)}[11]$. All other coefficients are set to 0.

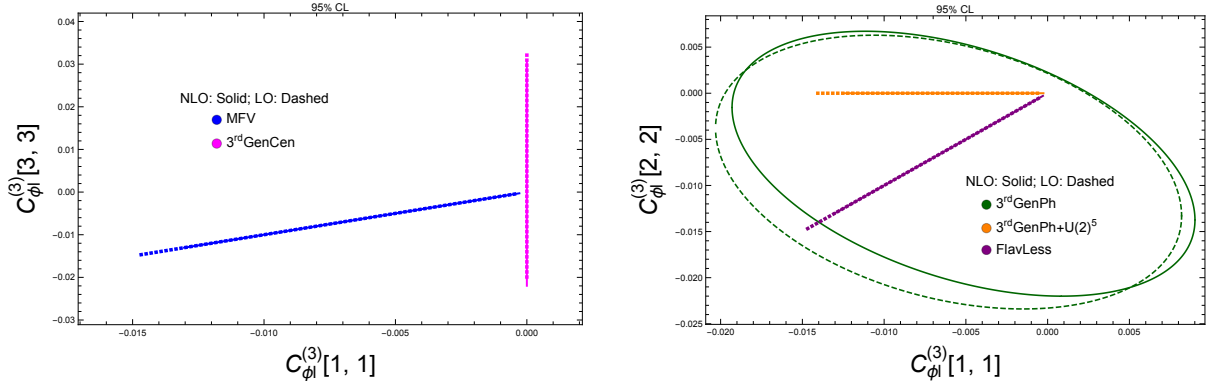


Figure 17. 95% CL limits on $C_{\phi_l}^{(3)}[ij]$ under flavor assumptions described in the text. Results at LO are drawn with dashed lines, results at NLO are drawn with solid lines. **On the left** we present $C_{\phi_l}^{(3)}[11]$ vs. $C_{\phi_l}^{(3)}[33]$ in the MFV (blue) and 3rd generation centric (magenta) scenarios. In these scenarios $C_{\phi_l}^{(3)}[22] = C_{\phi_l}^{(3)}[11]$. **On the right** we present $C_{\phi_l}^{(3)}[11]$ vs. $C_{\phi_l}^{(3)}[22]$ in the 3rd generation phobic (green), 3rd generation phobic + $U(2)^5$ (orange) and flavorless (violet) scenarios. In the first two scenarios $C_{\phi_l}^{(3)}[33] = 0$, while in the flavorless scenario $C_{\phi_l}^{(3)}[33] = C_{\phi_l}^{(3)}[22] = C_{\phi_l}^{(3)}[11]$. All other coefficients are set to 0.